Journal of Medicinal Chemistry

pubs.acs.org/jmc Article

Interrogating the Lactate Dehydrogenase Tetramerization Site Using (Stapled) Peptides

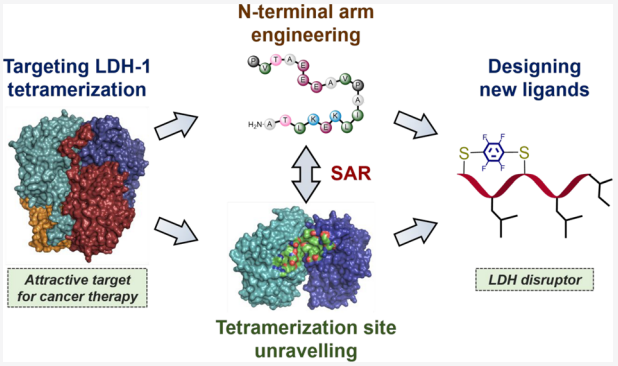
Léopold Thabault, Lucie Brisson, Chiara Brustenga, Santiago A. Martinez Gache, Julien R. C. Prévost, Arina Kozlova, Quentin Spillier, Maxime Liberelle, Zohra Benyahia, Joris Messens, Tamara Copetti, Pierre Sonveaux,* and Raphaël Frédérick*

Cite This: J. Med. Chem. 2020, 63, 4628−4643

Read Online

ACCESS | Metrics & More | Article Recommendations | Supporting Information

ABSTRACT: Lactate dehydrogenases (LDHs) are tetrameric enzymes of major significance in cancer metabolism as well as promising targets for cancer therapy. However, their wide and polar catalytic sites make them a challenging target for orthosteric inhibition. In this work, we conceived to target LDH tetramerization sites with the ambition of disrupting their oligomeric state. To do so, we designed a protein model of a dimeric LDH-H. We exploited this model through WaterLOGSY nuclear magnetic resonance and microscale thermophoresis for the identification and characterization of a set of α-helical peptides and stapled derivatives that specifically targeted the LDH tetramerization sites. This strategy resulted in the design of a macrocyclic peptide that competes with the LDH tetramerization domain, thus disrupting and destabilizing LDH tetramers. These peptides and macrocycles, along with the dimeric model of LDH-H, constitute promising pharmacological tools for the *de novo* design and identification of LDH tetramerization disruptors. Overall, our study demonstrates that disrupting LDH oligomerization state by targeting their tetramerization sites is achievable and paves the way toward LDH inhibition through this novel molecular mechanism.



INTRODUCTION

Cancer cells undergo tremendous metabolic adaptations in order to sustain their survival, anabolic growth, and proliferative agenda in environments that are often metabolically hostile. One of the distinctive features of their metabolic plasticity is the use of anaerobic and aerobic glycolysis, which switches energy production from oxidative phosphorylation (OXPHOS) to glycolysis. Anaerobic glycolysis allows cancer cells to survive under hypoxia when cellular respiration becomes problematic,[1] whereas aerobic glycolysis, also known as the Warburg effect,[2] redirects a fraction of the carbohydrate flux from energy production to anabolic pathways irrespective of oxygen availability, thereby promoting cell proliferation. Other cancer cells are more oxidative, consuming glucose, glutamine, lipids, and lactate as main metabolic substrates to fuel the tricarboxylic acid (TCA) cycle coupled to OXPHOS. These metabolic phenotypes are adaptive and generally interchangeable with space and time.

In many tumors, the net elevation of extracellular lactate levels, the end-product of glycolysis, drives pathogenesis by promoting several phenomena, including metabolic cooperation,[3] commensalism,[4] angiogenesis,[5−7] invasiveness,[8,9] and inflammation.[10,11] Moreover, a metabolic symbiosis can be established between oxidative and glycolytic cancer cells,[3] which further promotes autophagy through lysosomal acidification[12] and stabilizes the intracellular redox balance by controlling the NADH/NAD$^+$ ratio.[13]

At the core of lactate metabolism, lactate dehydrogenases (LDHs, EC 1.1.1.27), a family of NADH/NAD$^+$-dependent enzymes, catalyze the interconversion of pyruvate + NADH + H$^+$ to lactate + NAD$^+$. Functional LDHs are tetrameric enzymes constituted of two main subunits, LDH-M (encoded by the *LDHA* gene) and LDH-H (encoded by the *LDHB* gene), which can assemble in functional homo- and heterotetramers (LDH-1 to LDH-5) (Figure 1). Among these isoforms, homotetrameric LDH-1 (four LDH-H subunits) and homotetrameric LDH-5 (four LDH-M subunits) are the most extensively studied and are well-known for their implications in cancer cell proliferation and survival. *LDHA* is a hypoxia-inducible gene,[14,15] making of LDH-5 a key contributor to lactic fermentation in cancer. Conversely,

Received: November 25, 2019
Published: April 6, 2020



Downloaded via UNIV CATHOLIQUE DE LOUVAIN on May 31, 2020 at 01:23:22 (UTC).
See https://pubs.acs.org/sharingguidelines for options on how to legitimately share published articles.

ACS Publications © 2020 American Chemical Society

https://dx.doi.org/10.1021/acs.jmedchem.9b01955
J. Med. Chem. 2020, 63, 4628−4643

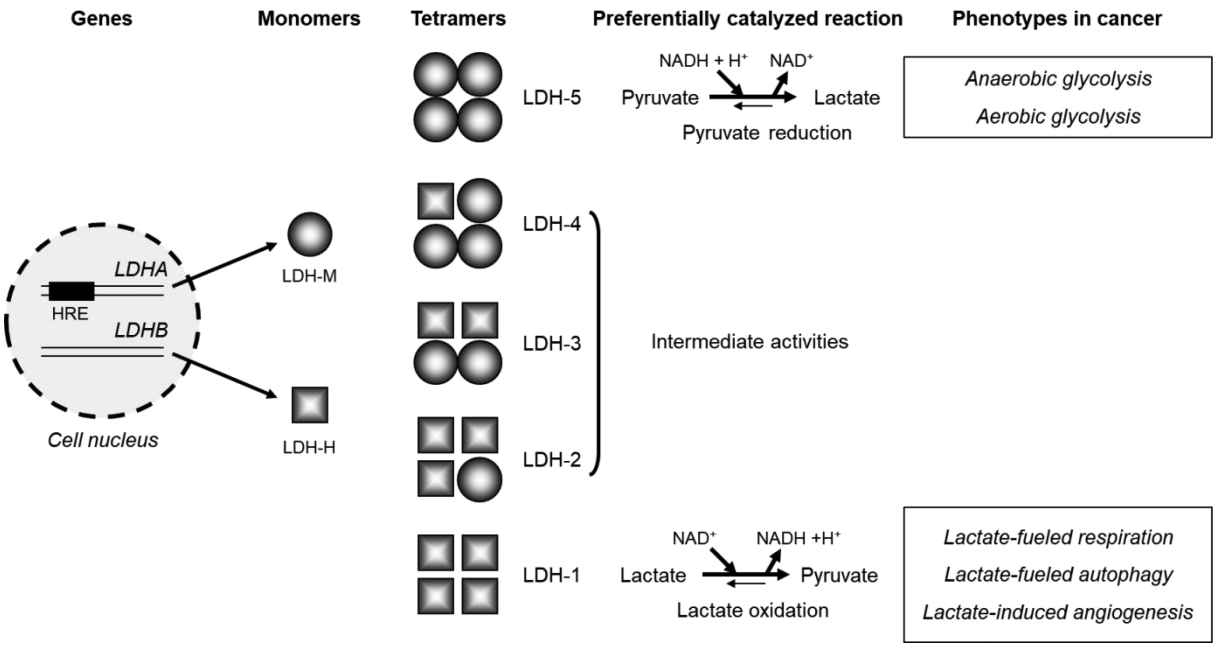


Figure 1. Nomenclature and functions of LDHs in cancer. In eukaryotic cells, *LDHA* and *LDHB* genes encode LDH-M and LDH-H monomers, respectively. Functional enzymes are tetramers formed by the arrangements of LDH-M and LDH-H subunits. LDH-5 (M_4) preferentially catalyzes the reduction of pyruvate to lactate in glycolytic cells. Owing to the presence of a hypoxia-responsive element (HRE) in its promoter region, *LDHA* gene expression is induced by hypoxia. In cancer, it accounts for lactate fermentation in cells performing either anaerobic or aerobic glycolysis. LDH-1 (H_4) preferentially catalyzes the oxidation of lactate to pyruvate in oxidative cells. In cancer, it accounts for lactate-fueled respiration and lactate-induced angiogenesis and promotes autophagy.

LDHB is predominantly expressed in oxidative cancer cells where LDH-1 facilitates lactate-fueled cancer cell respiration.[16] Despite sharing a high structural identity, LDH-1 and LDH-5 differ in their catalytic properties and subcellular localization. In physiological conditions, LDH-5 is predominantly found in glycolytic tissues, such as exercising skeletal muscles.[17] It has a higher affinity for pyruvate and NADH than for lactate and NAD^+, respectively, and a higher maximum velocity (V_{max}) for the reduction of pyruvate to lactate.[18−20] Comparatively, LDH-1 is mainly expressed in the heart, neurons, and red blood cells.[17] In physiological and pathological conditions, it has a better propensity to oxidize lactate to pyruvate, which can then fuel the TCA cycle.[18,19] Despite their physiological roles, LDH-1 and LDH-5 deficiency does not result in major pathological phenotypes in humans,[21,22] suggesting that long-term pharmacological inhibition of these proteins would only result in minor side effects.

The wide implication of LDHs in cancer pathogenesis makes them appealing targets for anticancer therapy.[23,24] During the past years, intense efforts have thus been devoted to develop small molecules able to selectively inhibit their activities.[24] However, despite the different catalytic properties between LDH-H and LDH-M, the catalytic site of the two subunits shares high structural homology (89% according to the NCBI basic local alignment search tool [BLAST]).[25] As a consequence, achieving selectivity for one isoform over the other is a challenging task with mitigated results.[26−28] Whether achieving selectivity between isoforms is desirable or not for cancer treatment is still under debate.[29] In fact, while some research groups focus on developing selective inhibitors, others argue for the potential additional therapeutic value of nonselective, pan-LDH inhibitors.[30,31]

So far, all molecules developed to inhibit LDHs focused on an interaction at the catalytic site and, therefore, suffered from common drawbacks due to the inherent structural features of LDH active sites that are highly polar and are mainly constituted by cofactor-binding sites.[13] As a result, most molecules interacting with LDH active sites are NAD^+-competitive and interact with the LDH "Rossman folds",[31,32] i.e., structural motifs shared by many dinucleotide-binding enzymes.[33] Most LDH inhibitors thus face a lack of selectivity for LDHs versus other NAD^+-dependent enzymes.[13] On the other hand, molecules that achieve potent interaction with LDH-H and LDH-M catalytic sites are usually hampered by their high polar nature and, hence, non-"drug-like" features, often resulting in poor *in cellulo* and *in vivo* activities.[31,32] Altogether, although LDHs are promising anticancer targets, LDH inhibitors have yet to demonstrate their potential in preclinical and clinical applications.

With the aim to set up a novel approach for more selective LDH inhibition, we decided to unravel and target LDH allosteric sites. Given that tetramers are the minimal functional units,[34,35] LDH activities rely on both their catalytic sites and oligomerization states. Targeting the oligomerization state of an enzyme is an emerging but underexplored strategy that has shown promising results during the past years.[36−39] Regarding LDHs, monomers are held together because of their N-terminal arms (also known as N-terminal domains) that extend from one monomer like an arm and wrap around two adjacent monomers, thus promoting the overall tetrameric cohesion.[40,41] Interestingly, the 33 and 32 amino acid N-terminal fragments of LDH-H and LDH-M, respectively, are known to interfere *in vitro* with the tetramerization of both isoforms.[42] These observations prompted us to evaluate this N-terminal arm as a starting point for the design and development of molecules interfering with LDH tetramerization.

https://dx.doi.org/10.1021/acs.jmedchem.9b01955
J. Med. Chem. 2020, 63, 4628−4643

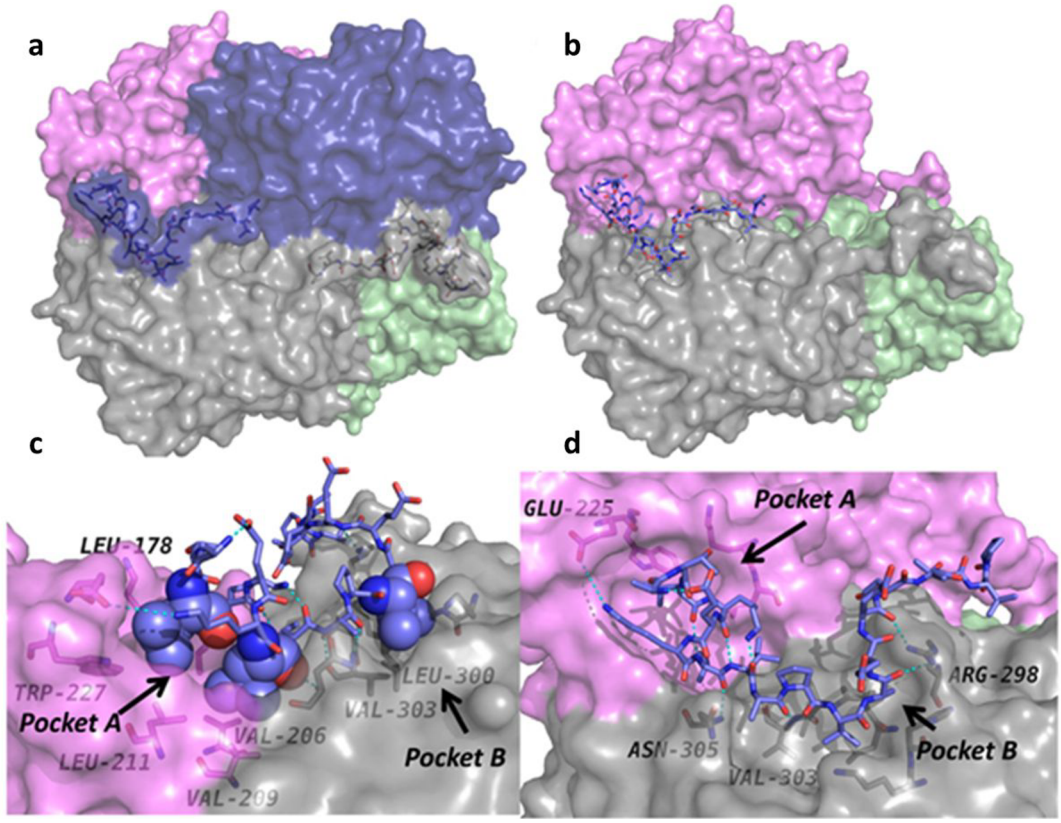


Figure 2. LDH-1 tetramer. Views of (a) full-length LDH-1 tetramer (PDB code 1I0Z) colored by monomer with the 19 N-terminal amino acids of the blue monomer shown by transparency, (b) **LB19** isolated from the blue monomer superimposed with the residual trimer where it interacts with the gray and pink monomers, and (c, d) main interaction sites (pockets A and B) between **LB19** and the two adjacent monomers (model realized using the Pymol software from Schrödinger).

RESULTS AND DISCUSSION

***In Silico* Study of the LDH Tetramerization Site.** Because LDH-M and LDH-H can hybridize *in vitro* and *in cellulo* to yield heterotetramers,[43] their tetramerization sites and N-terminal arms are structurally very close. Indeed, BLAST sequence alignment of the tetrameric sites of the two isoforms revealed 83% identity and 88% homology (Figure S1). We therefore did not expect to reach selectivity toward one subunit using our approach. Because LDH-1 simultaneously controls the oxidative metabolism of lactate, autophagy, and lactate signaling in cancer[3−11] (Figure 1), we focused our efforts on the N-terminal arm of human LDH-H. Analysis of the available LDH-1 crystallographic structure clearly showed the stabilization of the tetramer by interaction of the 19 N-terminal amino acid sequence of each monomer with two consecutive monomers, like four arms embracing the tetramer. These peptidic arms adopt a particular extended conformation, with a N-terminal α-helix followed by a short β-sheet connected to the monomer through a loop (Figure 2a,b). Comparing the four 19 N-terminal amino acids in the tetramer revealed slight differences regarding the orientations of the side chains, probably because of peptide flexibility. However, in all cases, the peptides did bind two adjacent pockets (A and B) on two different monomers, mainly via nonpolar interactions between residues Leu-3 and Leu-7 of the arm (amino acids shown with van der Waals [vdW] surface in Figure 2c) and Leu-178, Val-206, Val-209, Val-211, and Trp-227 in the A pocket, and Val-11 (also shown with vdW surface) and Leu-300 and Val-303 in the B pocket (Figure 2c,d). Polar interactions, such as hydrogen bonds (Ile-7 and Asn-305, Ala-9 and Val-303, Ala-12/Glu-14, and Arg298; Figure 2c,d), also contribute to the stabilization of the binding of the N-terminal arm of one subunit to the A and B pockets of two adjacent subunits.

On the basis of this structural analysis, we investigated the pharmacological properties of the human LDH-H 19 N-terminal amino acid peptide (ATLKEKLIAPVAEEEATVP), which we named **LB19**, on the full length LDH-1 tetramer. Unfortunately, enzymatic assays and biophysical evaluation showed no interaction between **LB19** and tetrameric LDH-1 (Figure S2a) or inhibition of tetrameric LDH-1 by **LB19** (Figure S2b). This lack of effect would stem from an "unfair" competition for the tetramerization site between the native N-terminal peptidic arm of LDH-H and the peptide **LB19**. To unravel the tetramerization site of the enzyme and better analyze this interaction, we decided to design and evaluate a new protein model.

Design and Evaluation of a Protein Model to Study LDH-H Tetramerization Site. To evaluate compounds targeting the LDH-1 tetramerization site, we produced a truncated version of human LDH-H that lacks its 19 N-terminal amino acids (LDH-Htr). We expected that, compared to full length tetrameric LDH-H (LDH-Hfl), LDH-Htr lacking its tetramerization arm would be in a native dimeric state and would therefore allow us to gain accessibility to its tetramerization site. Others indeed previously showed that a proteolysis of this N-terminal arm yields dimeric proteins.[41]

https://dx.doi.org/10.1021/acs.jmedchem.9b01955
J. Med. Chem. 2020, 63, 4628−4643

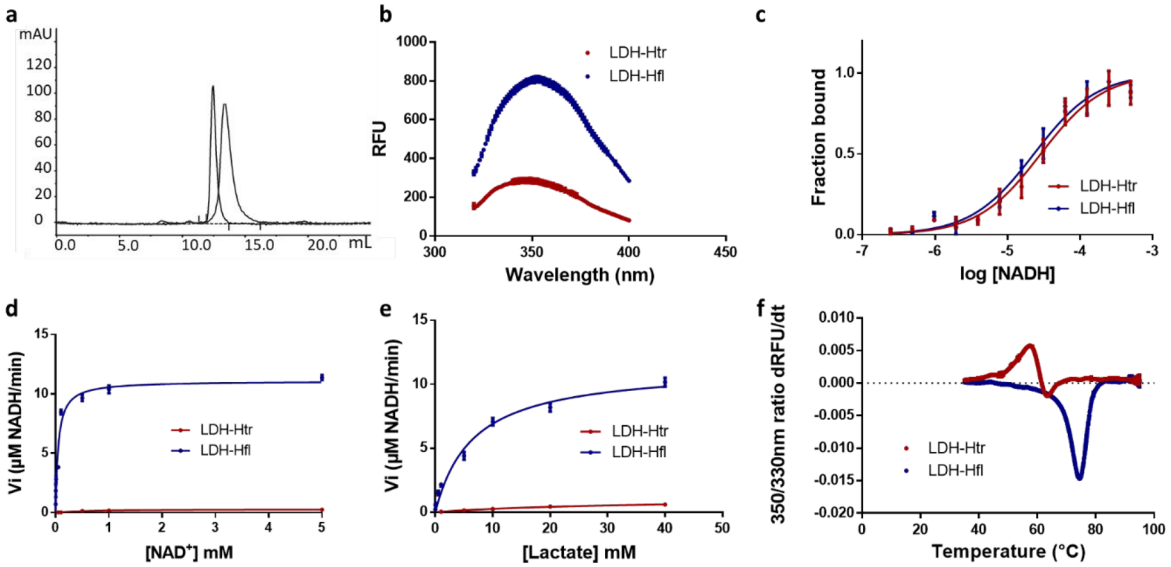


Figure 3. Compared to full length LDH-H that forms catalytically active tetramers, LDH-H truncated of its 19 N-terminal amino acids forms catalytically inactive dimers. (a–f) Comparison of full length (LDH-Hfl; blue) and truncated (LDH-Htr; red) LDH-H. (a) Overlay of size exclusion chromatograms of LDH-Htr (Rv = 12.45 mL, experimental MW = 78 kDa) and LDH-Hfl (Rv = 13.35 mL, experimental MW = 130 kDa). (b) Tryptophan fluorescence spectra of LDH-Htr (2.5 μM) and LDH-Hfl (2.5 μM). λ_{exc} = 286 nm (n = 6). (c) Evaluation of the K_d for NADH using microscale thermophoresis (MST) at a 10 s "on time" (n = 3). (d, e) Kinetic evaluation of LDH-Htr (7.7 nM) and LDH-Hfl (13.5 nM) at various lactate (d) and NAD^+ (e) concentrations (n = 6). (f) Nano differential scanning fluorimetry (nanoDSF) showing a melting temperature of 58 °C for LDH-Htr (15 μM) and of 75 °C for LDH-Hfl (15 μM) (n = 6).

LDH-Htr was recombinantly expressed in *E. coli* and was indeed found to be in a native dimeric state by size exclusion chromatography, with an experimental molecular weight (MW) of 78 kDa (theoretical MW = 73 kDa) (Figure 3a). Tryptophan fluorescence showed a strong decay of intensity, as well as a blue shift for LDH-Htr compared to LDH-Hfl (Figure 3b) due to solvent exposure of tryptophan residues, as suggested by Opitz et al.[34] The affinity of LDH-Htr for NADH was evaluated using microscale thermophoresis (MST), and a K_d of 28.8 μM [$CI_{95\%}$ of 25.1 μM to 33.1 μM] was obtained, similar to the one obtained for the full length tetrameric LDH-1 (LDH-Hfl) (23.2 μM [$CI_{95\%}$ of 19.5 μM to 27.6 μM]) (Figure 3c), suggesting a correct folding of the Rossman fold. The catalytic properties of LDH-Htr were also evaluated using standard enzyme kinetic experiments following NADH formation and showed a very weak activity in comparison with LDH-Hfl, with a 3 to 20-fold increase in Michaelis–Menten constant K_M as well as a 10-fold decrease in maximal velocity V_{max} for both the substrate lactate and the cofactor NAD^+ (Figure 3d,e and Table 1). LDH-Htr stability was evaluated using nano differential scanning fluorimetry (nanoDSF) (Figure 3f). Dimeric LDH-Htr was very unstable when compared to its tetrameric counterpart, with a difference of 17 °C in melting temperature. Altogether, these results revealed that LDH-Htr is a well folded but poorly active dimeric protein. They also confirmed that targeting LDH-1 tetramerization could destabilize the enzyme and almost totally abolish its catalytic activity.

Table 1. Kinetic Properties of Full Length and Truncated LDH-H[a]

	truncated LDH-H	full length LDH-H
K_M NAD^+(mM)	0.587 ± 0.057	0.208 ± 0.005
K_M lactate (mM)	33.77 ± 6.17	1.686 ± 0.284
V_{max} ($\mu M \cdot s^{-1}$)	0.0122 ± 0.003	0.190 ± 0.012
k_{cat} (s^{-1})	0.906 ± 0.009	24.00 ± 1.51

[a]Reported values are the mean ± SEM for n = 6.

Study and Optimization of the Interaction between LB19 and the LDH-H Tetramerization Site. In order to evaluate whether LDH-Htr had unraveled the LDH-H tetramerization site, we characterized the interaction between **LB19** and LDH-Htr. Biophysical evaluation was performed using two orthogonal biophysical methods: MST and NMR WaterLOGSY.[44] According to the MST analysis, **LB19** interacts with LDH-Htr with a K_d of 1.78 mM [1.14–2.77 mM] (Figure 4a). In agreement, NMR WaterLOGSY analysis revealed a saturation transfer stemming from an interaction between **LB19** and LDH-Htr (Figure 4b). Moreover, careful inspection of NMR WaterLOGSY spectra combined with two-dimensional NMR-TOCSY analysis allowed for epitope mapping of the interaction between the **LB19** and LDH-Htr (Figure 4b,c and Table S1). Interestingly, **LB19** N-terminal residues underwent more saturation transfer than C-terminal residues (Figure 4b), suggesting that **LB19** N-terminal residues account for most of the binding strength. In accordance with this observation, sequence alignment of the N-terminal parts of LDH-H of human and other vertebrates showed a strong conservation of these residues, whereas C-terminal residues were more variable (Figure 4d). Computational prediction of the overall binding energy of LDH-H native arm further supported these results, as most of the predicted free energy of binding was located in the N-terminal region (Figure S3).

Following these observations, we decided to progressively trim the C-terminal end of LB19 in order to keep only the residues of the N-terminal end accounting for the binding of the peptide to LDH-Htr. We first evaluated a shorter peptide constituted of **LB19** 13 N-terminal amino acids (ATLKE-KLIAPVAE), which we named **LB13**. **LB13** contained all the interacting residues and, as expected, presented the exact same

https://dx.doi.org/10.1021/acs.jmedchem.9b01955
J. Med. Chem. 2020, 63, 4628–4643

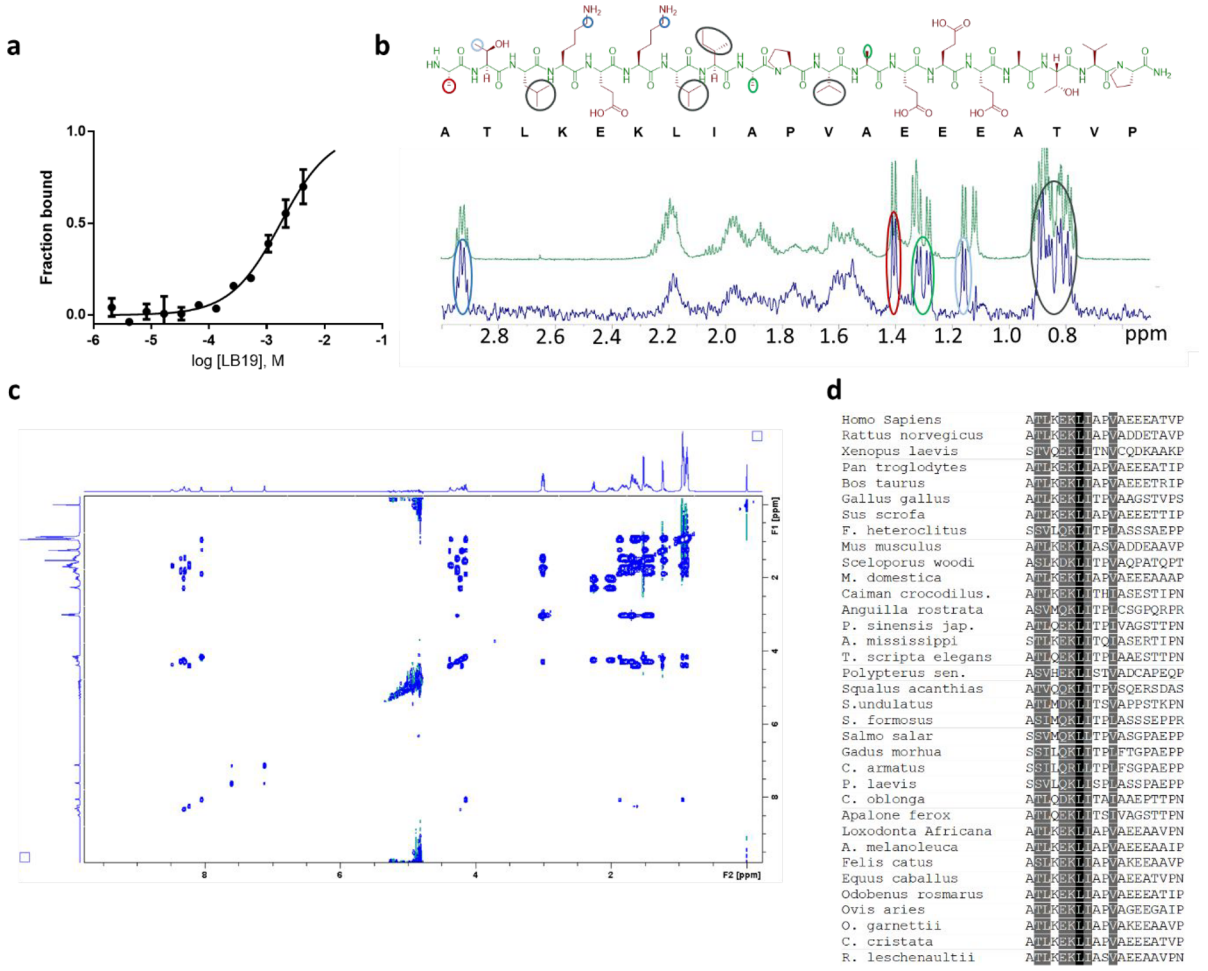


Figure 4. Characterization of the binding of **LB19** to LDH-Htr. (a) Binding curve of **LB19** on LDH-Htr providing a K_d of 1.78 mM [1.14−2.77 mM]. Binding curve was extracted from the MST traces at a 10 s MST on time (n = 3). (b) Traces show the one-dimensional NMR ^{1}H proton spectrum of **LB19** (green) overlaid with its corrected NMR WaterLOGSY spectrum (blue) at 800 μM. Circled positive signals on the spectra are matched to the corresponding interacting residues in the formula of the peptide shown above. Peptide backbone is displayed in green and side chains in red. (c) **LB19** two-dimensional TOCSY spectrum used to get full **LB19** assignment. Complete assignment of **LB19** ^{1}H spectrum can be found in Table S1. (d) LDH-H tetramerization arm sequence alignment of several vertebrates. Black and gray residues represent a 100% identity and a 100% similarity, respectively.

NMR WaterLOGSY spectrum as **LB19** (Figure 5). Moreover, MST analysis confirmed that the interaction was not significantly different from **LB19**, with a K_d of 1.02 mM [0.53−1.99 mM].

Further trimming **LB13** led to **LB8** (ATLKEKLI), which, apart from a valine residue that was removed in position 11, contained the same interacting residues as **LB13**. We observed no significant loss of the binding potency of the peptide to LDH-Htr (K_d = 1.05 mM [0.55−2.01 mM]). **LB8** exactly matched with the N-terminal α-helix of the LDH-H tetramerization arm and, therefore, can be considered as a "hot spot" of the interaction. A **LB19** central fragment (LIAPVAE, which we named **LBc**) demonstrated no appreciable saturation transfer under these conditions and was used as a negative control. Importantly, NMR WaterLOGSY evaluation of **LB19** and **LB8** against tetrameric LDH-1 yielded no appreciable binding, suggesting that the observed signal was stemming from a specific interaction occurring at the LDH-H tetramerization site (Figure S4). Of further note, evaluation of the eight N-terminal amino acids of LDH-M (ATLKDQLI), which we named **LA8**, showed a similar NMR WaterLOGSY spectrum and binding affinity to LDH-Htr than **LB8**, with a K_d of 1.49 mM [1.14−1.94 mM]. This observation is coherent with the fact that LDH-H and LDH-M can form stable heterotetramers.[45]

Unravelling LB8 and LDH-H Tetramerization Arm "Hot Spots". We next aimed to determine the structure−activity relationship (SAR) of **LB8** binding to the LDH-H tetramerization site. As the interacting conformation of **LB8** was expected to be a short α-helix, a combination of orthogonal experimental evaluations was used to unravel LB8 SAR. To identify structural modifications that would result in a loss of saturation transfer, we performed single amino acid substitutions on **LB8**. We therefore tested a set of 12 **LB8** structural analogues by NMR WaterLOGSY experiments, at a concentration of 800 μM (Figure 6a). In agreement with the analysis of the crystallographic data, Leu3 and Leu7 were found to be required for the binding, as their replacement with alanine or glycine led to a loss of interaction. The *in silico* representation of **LB8** extracted from the LDH-H crystallographic structure indicates that these aliphatic side chains project toward hydrophobic cavities at the tetramerization site (Figure 6b). A careful integration of LB8 NMR WaterLOGSY spectra confirmed that lipophilic residues undergo more

https://dx.doi.org/10.1021/acs.jmedchem.9b01955
J. Med. Chem. 2020, 63, 4628−4643

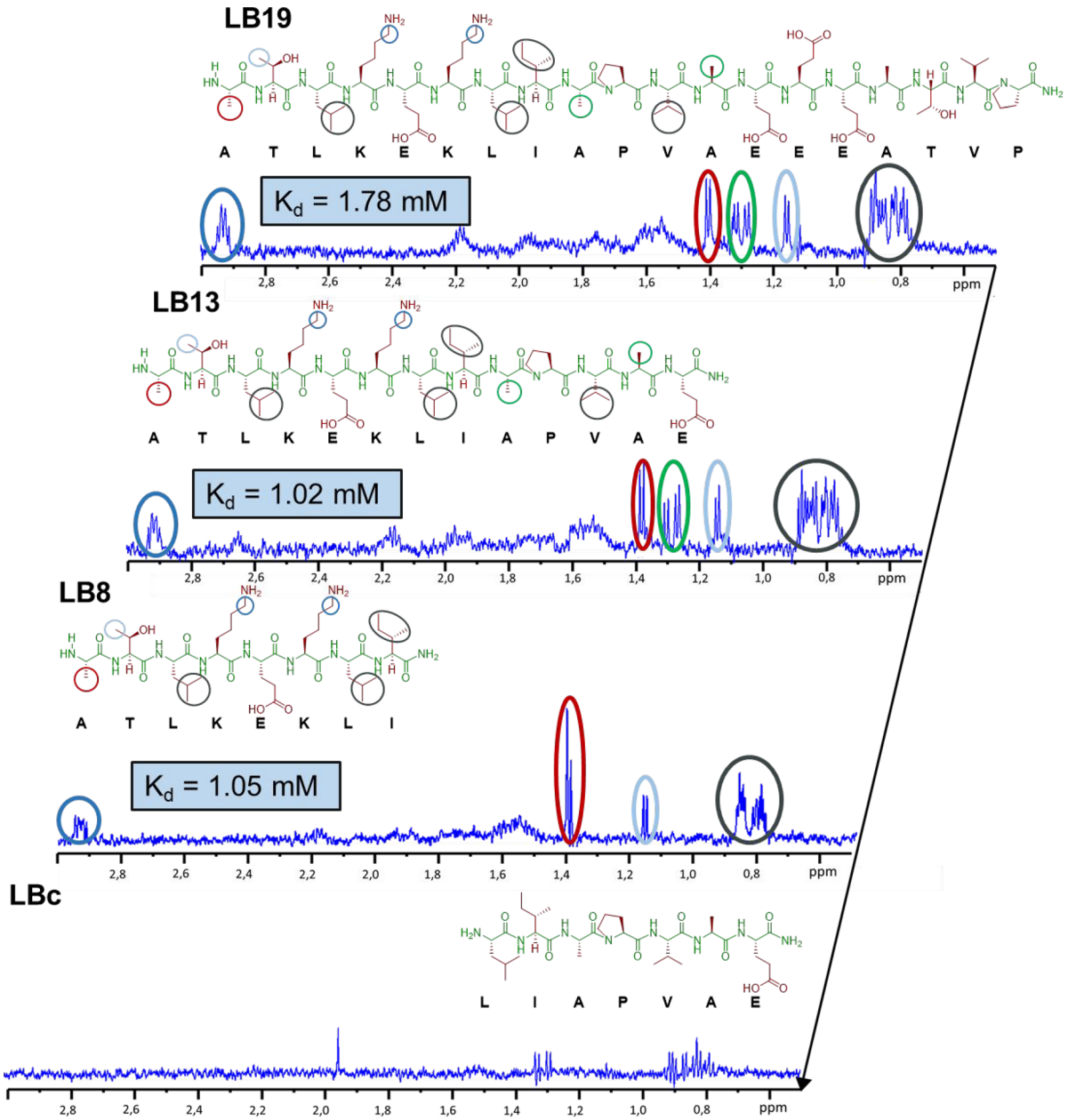


Figure 5. Optimization of small peptides binding to the LDH-H tetramerization site. Corrected aliphatic region WaterLOGSY spectra of **LB19** and its shorter derivatives **LB13** and **LB8** at 800 μM with LDH-Htr (15 μM). Circled positive signals on the spectra are matched to the corresponding interacting residues in formulas. The **LBc** spectrum, used as a negative control, shows no saturation transfer under similar conditions. Dissociation constants (K_d) were extracted from the MST traces at a 10 s MST on time (n = 3). Complete assignment of LB19, LB13, and LB8 ^{1}H spectrum are respectively in Tables S1, S2, and S3.

saturation transfer than any of the others, thus interacting more closely with the tetramerization site (Figure 6c). Removal of any of the terminal residues resulted in an abrogation of the interaction (Figure 6a). We therefore reasoned that trimming **LB8** to get shorter peptides would result in a destabilization of its short α-helix conformation. Accordingly, circular dichroism measurements confirmed that heptapeptides ATLKEKL and Ac-TLKEKLI presented a lesser helix propensity than their full-length counterpart (Figure S5a). Still, **LB8** helical propensity in water was already very low, as confirmed by circular dichroism (Figure S5b) and two-dimensional ROESY NMR (Figure S5c). Such a poor helical folding can be responsible for the weak potency of **LB8** and suggests that a conformational stabilization could increase its potency. Modifications of other residues had no impact on the interaction of the peptide with the LDH-H tetramerization site.

In order to validate the hot spots, we performed a single amino acid substitution to alanine on the eight N-terminal amino acids of LDH-Hfl. The seven variants were tested for their capacity to oligomerize and for their stability using a guadinidium·HCl (Gdn.HCl) dissociation assay,[46] nanoDSF, and size exclusion chromatography (SEC). Strikingly, LDH-H^{L7A} was the most unstable variant, as it was only found in a dimeric state by SEC and therefore never formed tetramers (Table 2). Consistently, its DSF pattern (Figure 7a) and its intrinsic fluorescence spectrum (Figure S6) matched the ones of LDH-Htr. Replacing either Leu3 or Ile8 by alanine also deeply reduced the stability of the resulting LDH-H^{L3A} and

https://dx.doi.org/10.1021/acs.jmedchem.9b01955
J. Med. Chem. 2020, 63, 4628−4643

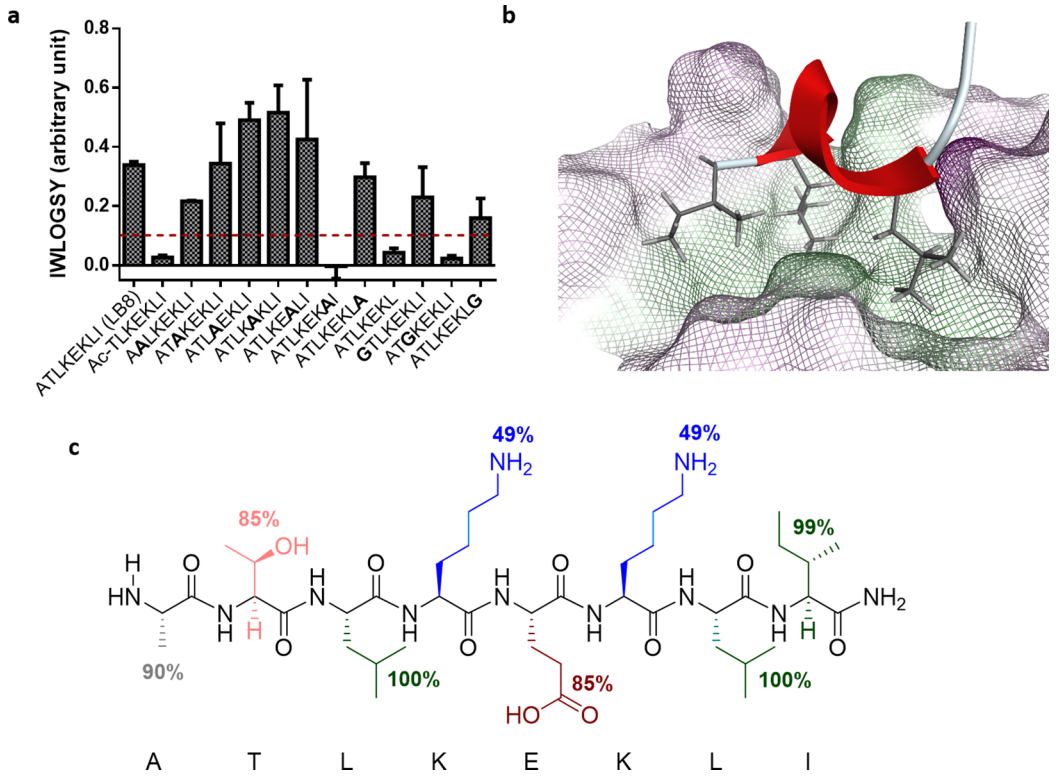


Figure 6. Structure−activity relationship of **LB8** binding to LDH-Htr. (a) Screening **LB8** analogues at 800 μM for their binding to LDH-Htr (15 μM) using a NMR WaterLOGSY sequence. The red dotted line represents a threshold of 0.1 corresponding to a 10% increase in WaterLOGSY signal when compared to control experiment. Displayed data are obtained from 512 accumulations (n = 2). (b) *In silico* model of the interaction of **LB8** with the LDH-H tetramerization site extracted from the available crystallographic structure (PDB entry 1I0Z, pictures made using the MOE software from ChemComp). **LB8** is pictured as a red α-helix, and only its lipophilic residues projecting toward the tetramerization site are displayed. van der Waals surface is represented as a mesh and colored in green and purple for lipophilic and polar environments, respectively. (c) Saturation transfer intensity of **LB8** residues at 1 mM from NMR WaterLOGSY experiments resulting from 2048 accumulations at 4 °C. Experimental intensities are normalized to the residues presenting the highest saturation transfer.

Table 2. Oligomeric State and Stability of LDH-H Variants[a]

	retention volume (mL)	experimental MW (kDa)	melting temperature (°C)	EC_{50} of tetrameric disruption over GdN.HCl exposure (M)
LDH-H	14.01	124	74.5 ± 0.1	1.112 ± 0.012
LDH-Htr	14.50	96	57.5 ± 0.2	
LDH-H^{T2A}	13.88	134	72.37 ± 0.1	0.978 ± 0.012
LDH-H^{L3A}	13.78	141	61.2 ± 0.1	0.624 ± 0.013
LDH-H^{K4A}	13.84	137	65.8 ± 0.1	0.991 ± 0.006
LDH-H^{E5A}	13.85	136	73.3 ± 0.1	1.010 ± 0.009
LDH-H^{K6A}	13.81	138	67.9 ± 0.1	0.954 ± 0.007
LDH-H^{L7A}	14.55	93	55.6 ± 0.1	
LDH-H^{I8A}	13.92	131	49.9 ± 0.1	0.233 ± 0.027

[a]Reported values are the mean ± SEM (n = 6 for melting temperatures and n = 3 for EC_{50}).

LDH-H^{I8A}, with a ΔT_m of 13.3 and 24.6 °C, respectively, compared to LDH-Hfl. Similar results were observed with the study of their oligomeric stability upon Gdn.HCl exposure (Figure 7b and Table 2). Other amino acid replacements had little to no impact on the LDH-1 tetrameric stability and oligomerization state. NanoDSF showed that LDH-H^{K4A} and LDH-H^{K6A} were slightly destabilized, but the thermal shift most probably reflected a difference in the partial charge of the protein, as oligomeric stability over Gdn.HCl exposure was not impacted (Figure 7a,b and Table 2). Overall, the impact of these single amino acid substitutions of the tetramerization arm of LDH-H coherently matched with the SAR of **LB8**, with lipophilic residues being key elements for interaction. However, switching isoleucine to alanine had a much more destabilizing effect on the LDH-H^{I8A} oligomeric stability (Figure 7a) than on the ability of **LB8**^{I8A} or **LB8**^{I8G} to bind to the tetramerization site of LDH-Htr (see Figure 6a), as the switch of isoleucine to alanine or glycine only slightly weakened the saturation transfer of ATLKEKLA or ATLKEKLG with LDH-Htr. Such a difference of profile can be accounted for by a modest difference of the conformation of the octapeptide compared to the native arm, as Ile8 is located at the hinge region between the N-terminal α-helix and the following short β-strand of LDH-H. A summary of **LB8** SAR obtained in the light of our orthogonal approaches is displayed in Figure 7c.

Constraining LB8 to Stabilize Its Active Conformation. We then hypothesized that the weak binding of **LB8** to LDH-Htr could be due to its poor helical propensity that would result in a significant entropy cost prior to binding. As previously mentioned, NMR 2D ROESY analysis confirmed the absence of the α-helix characteristic cross coupling in the NH region of the peptide (Figure S5c). Consistently, circular dichroism measurements displayed only random coil in aqueous conditions (Figure S5b). In order to increase helicity, we first introduced α-methylalanine (Aib), a known helicogenic residue at positions 4 and 6 of **LB8**, two positions identified as nonessential for the interaction of **LB8** with LDH-

https://dx.doi.org/10.1021/acs.jmedchem.9b01955
J. Med. Chem. 2020, 63, 4628−4643

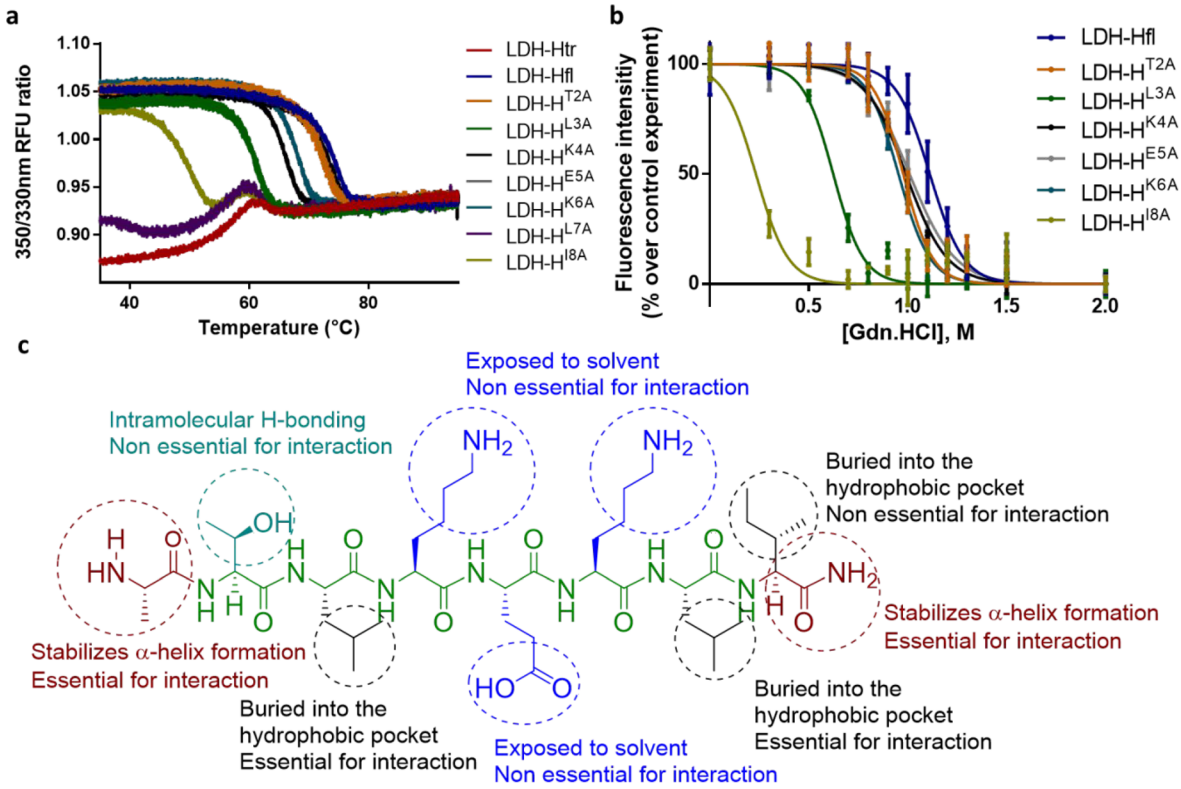


Figure 7. An alanine scan on the eight N-terminal amino acids of the LDH-H tetramerization arm unravels key residues for tetramerization. (a) Screening of LDH-H variants using nanoDSF. Changes in the 350/330 nm fluorescence emission indicate blue or red shifts and are representative of unfolding events (n = 6). (b) Dissociation of the homotetrameric form of LDH-H and of its variants at 50 μg/mL (1.3 μM) upon addition of guanidinium·HCl. Tryptophan fluorescence intensity was followed at λ_{exc} = 286 nm, λ_{em} = 350 nm as a direct reporter of LDH-1 tetrameric integrity[46] (n = 3). (c) Overall **LB8** structure−activity relationship according to amino acid scans on **LB8** and LDH-H and crystallographic data.

Htr. While the resulting peptides **LB8**$^{(K4Aib)}$ and **LB8**$^{(K6Aib)}$ still interacted with LDH-Htr as detected by NMR WaterLOGSY, no improvement of the K_d was observed by MST. NMR 2D ROESY analysis further confirmed the absence of helicity for these two peptides (Figure S7).

Our second approach to promoting the helicity of **LB8** involved peptide macrocyclization. In fact, previous studies of unrelated peptides have shown that an entropy-mediated gain in potency can be achieved by constraining the conformational freedom of peptides.[47] We therefore decided to perform a **LB8** side chain to side chain cyclization in order to promote its helicity. Many strategies have been described for peptide macrocyclization.[47] Among them, cysteine stapling with an α-helix-promoting agent already demonstrated strong results in enhancing small peptide helicity (Figure 8a) and hence affinity for their targets.[48] On the basis of **LB8** SAR, we introduced cysteines at various i and i + 4 positions and cross-linked these peptides using α,α'-dibromo-m-xylene.[48] The resulting cyclic peptides **1**−**6** were then evaluated for their binding to LDH-Htr using MST (Table 3).

SAR of the synthesized macrocycles revealed a strong influence of the linker position (Figure 8b). In accordance with our *in silico* model, only macrocyclization of solvent-exposed i and i + 4 residues yielded interacting cyclic peptides. The size of pocket A appeared moreover to disadvantage the interaction of a longer α-helix (Figures 2a and S8a). Among interacting molecules, macrocycle **1** (Figure 8c), resulting from a stapling between positions 1 and 5, appeared to be the most promising binder with an apparent 17-fold increase in potency (K_d = 64 μM) compared to **LB8** (K_d = 1.05 mM) (Figure 8d). Circular dichroism analysis revealed a strong increase in the θ_{206} band, as well as a more modest one at θ_{222} for macrocycle **1** when compared to unconstrained peptide **LB8** (Figure 8e), consistent with the expected increase in α-helicity.

Following identification of the optimal i and i + 4 position for **LB8** cyclization, we investigated macrocyclic peptides bearing other linkers (Table 3), including p-tetrafluorophenyl (**7**), o-benzyl (**8**), p-benzyl (**9**), as well as a lysine to aspartate lactam bridge between the side chains of the K_1 and D_5 residues (**10**).[49] Strikingly, K_d evaluation of these macrocyclic peptides revealed a strong impact of the overall constrain imposed by the linker on the evaluated affinity. Indeed, p-tetrafluorophenyl (**7**) and o-benzyl (**8**) analogues yielded a supplementary 2- to 6-fold improvement in affinity when compared to macrocycle **1**, with K_d's of 11 and 25 μM, respectively. Comparatively, less constraining linkers, p-benzyl (**9**) and the K_1-D_5 lactam bridge (**10**), resulted in weakly potent derivatives with K_d's of 113 and 142 μM, respectively.

We further investigated the influence of a lactam bridge between the N-terminal amino group and the carboxylic acid on the side chain of the E_5 residue, as these two moieties can be found close to each other in **LB8** *in silico* model (Figure S8b). The resulting macrocycle **11** was found to be slightly more potent than **LB8**, with a K_d of 465 μM. For comparison, we also evaluated the impact of a lactam bridge between K_6 side-chain NH_2 and the C-terminal carboxylate. The resulting peptide **12** yielded no appreciable binding using either NMR or MST.

Destabilizing and Disrupting LDH Tetramerization with Designed Macrocyclic Peptides. Finally, we tested

https://dx.doi.org/10.1021/acs.jmedchem.9b01955
J. Med. Chem. 2020, 63, 4628−4643

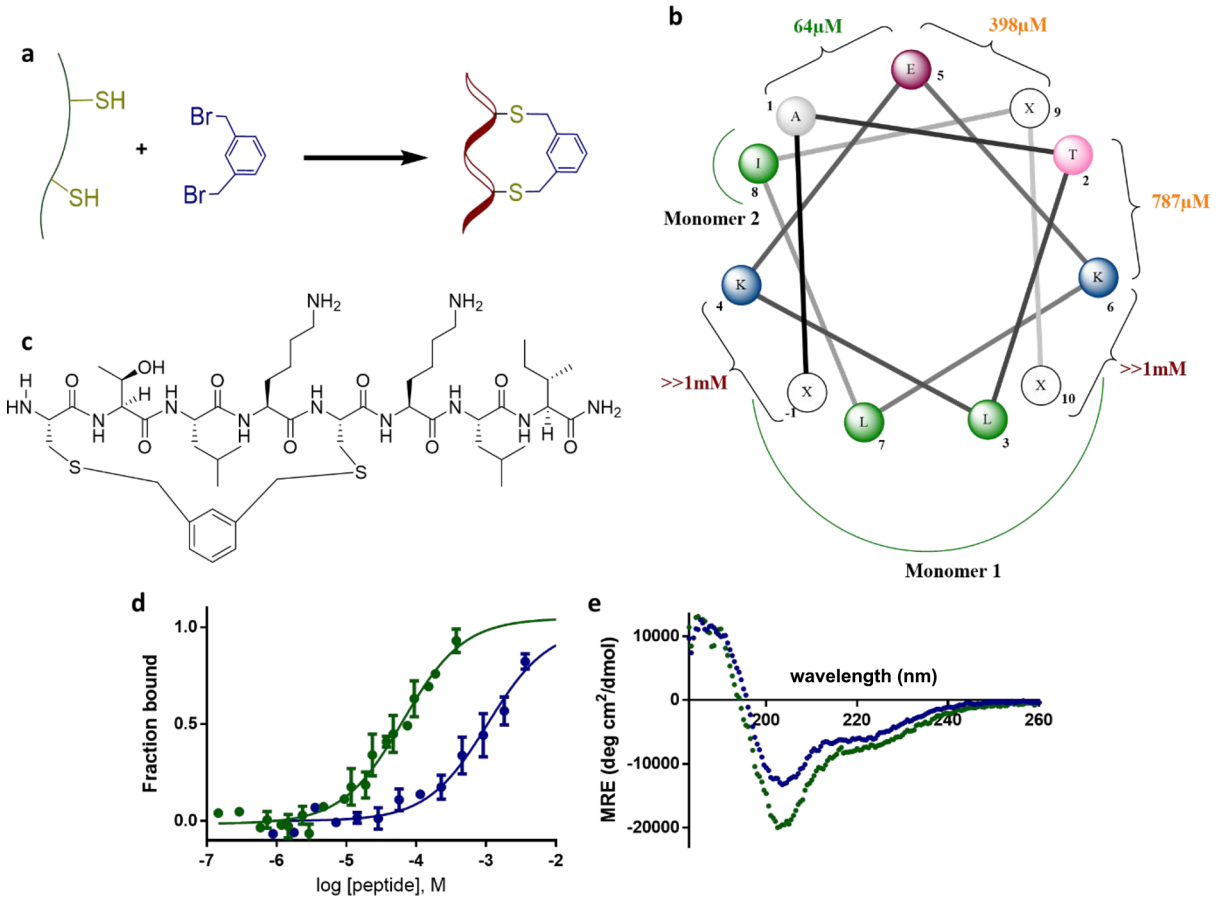


Figure 8. Synthesis and evaluation of cyclic peptides targeting the LDH-H tetramerization site. (a) Schematic representation of the cysteine stapling strategy used to promote helicity. (b) Helical wheel projection of **LB8**-derived peptides and their positions compared to the LDH-H tetramerization site. Reported values correspond to K_d's of the cyclic peptides resulting from the cross-linking of residues between the corresponding brackets. Apolar residues are colored in green, polar neutral in pink, acidic in purple, and basic in blue. (c) Structure of macrocycle **1**. (d) Comparison of the binding curves of macrocycle **1** (green) (K_d = 64 μM) and **LB8** (blue) (K_d = 1.05 mM) on LDH-Htr obtained by MST. Binding curves were extracted from the MST traces at a 10 s MST on time (n = 3). (e) Circular dichroism spectra of linear **LB8** (blue) compared to macrocycle **1** (green). Experimental conditions: ~100 μM peptide, 10 mM sodium phosphate (pH 7.6), 20% TFE.

Table 3. Code, Structure, Dissociation Constant (K_d), and 95% Confidence Interval of Evaluated Macrocycles against Truncated LDH-H[a]

molecule	sequence	linker	K_d[a]	$CI_{95\%}$
LB8	ATLKEKLI		1.05 mM	0.55−2.01 mM
1	CTLKCKLI	*m*-benzyl	64 μM	55−75 μM
2	ACTLKCKLI	*m*-benzyl	67 μM	55−82 μM
3	ACLKECLI	*m*-benzyl	787 μM	529−1171 μM
4	ATLKCKLIC	*m*-benzyl	398 μM	246−645 μM
5	ATLKECLIAC	*m*-benzyl	≫1 mM	ND
6	CATLCEKLI	*m*-benzyl	≫1 mM	ND
7	CTLKCKLI	*p*-tetrafluorophenyl	11 μM	9−14 μM
8	CTLKCKLI	*o*-benzyl	25 μM	21−29 μM
9	CTLKCKLI	*p*-benzyl	113 μM	98−131 μM
10	Ac-KTLKDKLI	lactam bridge K_1-D_5	142 μM	117−174 μM
11	ATLKEKLI	lactam bridge Nter-E_5	465 μM	355−607 μM
12	ATLKEKLI	lactam bridge K_6-Cter	≫1 mM	ND

[a] K_d values were extracted from MST traces at 10−20 s on time (n = 3 for macrocycles **1**−**4** and **7**−**11**, n = 2 for macrocycles **5**, **6**, and **12**). ND, not determined.

whether macrocyclic peptides **1** and **7** were able to compete with N-terminal domain of native LDH-H. To this end, we first investigated their ability to interact with tetrameric LDH-1 and LDH-5 using MST. Interestingly, compound **7**, the most potent analogue, displayed an interaction at high concentrations with LDH-1 and LDH-5 (Figure 9a) with estimated K_d's of 380 μM ($CI_{95\%}$ of 315−457 μM) and 117 μM ($CI_{95\%}$ of 94−144 μM), respectively. Comparatively, macrocycle **1** did

https://dx.doi.org/10.1021/acs.jmedchem.9b01955
J. Med. Chem. 2020, 63, 4628−4643

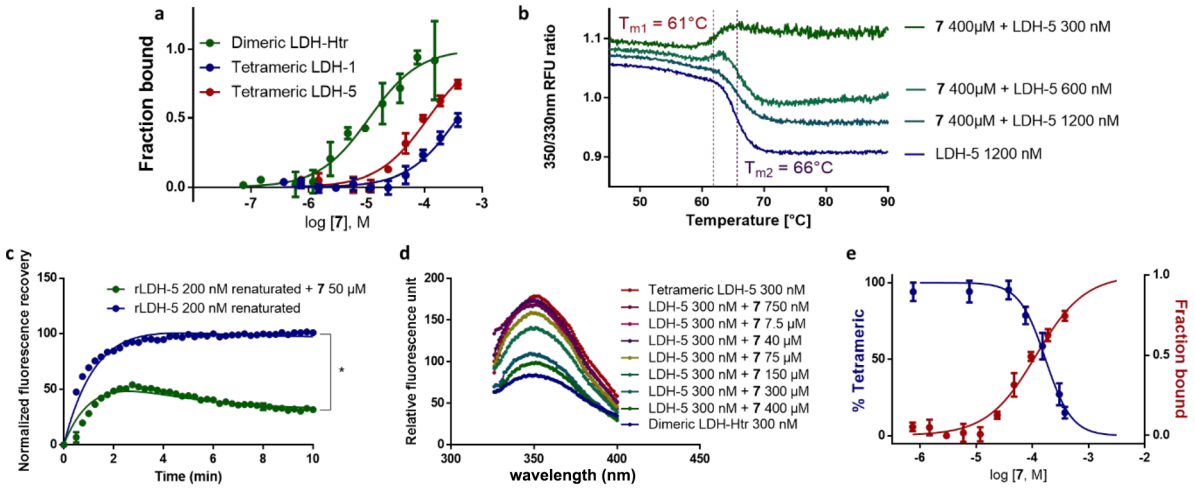


Figure 9. Designed macrocycle **7** can inhibit LDH association, destabilize, and disrupt tetrameric human LDHs. (a) MST binding curves of macrocycle **7** on dimeric LDH-Htr (green), tetrameric LDH-1 (blue), and LDH-5 (red). Binding curves were extracted from MST traces at a 10−20 s on time (n = 3) except for the binding curve with LDH-5 which was extracted from the red-dye raw fluorescence (n = 3). (b) NanoDSF of various concentrations of human LDH-5 exposed to macrocycle **7** (n = 6). Changes of the 350/330 nm fluorescence emission indicate blue or red shifts and are representative of unfolding events. (c) Impact of **7** on LDH-M fluorescence recovery after acidic exposure (n = 6). (d) LDH-5 tryptophan fluorescence spectra upon increasing concentration of **7** (n = 8, one experience in quadruplicate is displayed, another can be found in Figure S11h). (e) Tetrameric state of LDH-5 upon increasing concentration of **7** (blue) overlayed with the binding curve of **7** with LDH-5 obtained from MST (red). The tetrameric state is estimated using the 350 nm fluorescence intensity normalized in regard to the spectra of LDH-5 (considered as 100% tetrameric) and LDH-Htr (considered as 0% tetrameric). For clarity, SEMs are not represented on graphs (b) and (d) but can be found in Figures S10b−e and S11h,i respectively.

not demonstrate any binding in similar conditions (Figure S9). This interaction between **7** and the tetrameric protein thus suggested a displacement of LDH N-terminal arm by the cyclic peptide to reach for the tetramerization site.

We further investigated the ability of macrocycles **1** and **7** to destabilize tetrameric LDH-1 and LDH-5. Indeed, molecules interacting at oligomeric interfaces can reduce the melting temperature of the studied oligomers owing to a perturbation of the overall stability of the complex.[50,51] We therefore evaluated the impact of macrocycles **1** and **7** on LDH-1 and LDH-5 thermal denaturation using nanoDSF. While **1** had no effect up to 500 μM on both human LDH-1 and LDH-5 stabilities (Figure S10a), macrocycle **7** induced a destabilizing conformational change on both isoforms at 400 μM (Figures 9b and S10b−e). As LDH-5 is less stable than LDH-1 (Figure S10f), the destabilization was stronger on the LDH-5 tetramer (ΔT_m = −5 °C) than on LDH-1 (ΔT_m = −1.5 °C). Of note, this difference in stability of the two isozymes probably accounts for the higher affinity of **7** to LDH-5 as observed by MST. The intensity of the effect was moreover dependent on protein concentration, which is coherent with the hypothesis that an increasing amount of monomers would result in a shift of the equilibrium toward the formation of tetrameric complexes. Of note, macrocycle **7** did not induce such destabilization against our dimeric model of LDH (Figure S11a).

We next evaluated whether these macrocyclic peptides could also bind to the tetramerization site during LDH tetramer formation. Such an approach was already reported, for instance, in the case of peptides interacting at the interface of human glutathione reductase.[37,52]

We thus designed an experiment to follow the recovery of LDH tetramers after a dissociation step initiated by acidic conditions. These experiments were conducted on LDH-5, as it is less stable and thus more prone to dissociation than LDH-1.[53] Because strong acidic conditions (pH 2.3) are necessary to disrupt the human LDH-5 (hLDH-5) homotetramer,[54] which results in partial protein denaturation, we set to work on rabbit LDH-5 (rLDH-5) that dissociates at less acidic conditions (pH 5),[55] does not denaturate, and affords reproducible data. rLDH-5 shares 94% sequence identity and 98% homology with the hLDH-5, with similar nanoDSF denaturation patterns (Figure S11b). Monitoring of the rLDH-5 tetrameric state was performed by following its intrinsic tryptophan fluorescence: six tryptophan residues can be found in each rLDH-M monomer, three of them being located at the dimer−dimer interface. As the tryptophan quantum yield decreases in a polar environment, dimeric LDHs show very weak tryptophan fluorescence compared to the tetrameric form.[34] Accordingly, dimeric rLDH-M showed very weak tryptophan fluorescence at pH 5 when compared to the high fluorescence of tetrameric rLDH-5 at pH 7.6 (Figure S11c). Such decay can be compared to the difference in tryptophan fluorescence between tetrameric LDH-1 and dimeric LDH-Htr (Figure 3b).

When neutral pH was restored following acidification, macrocycles **1** and **7** significantly interfered with LDH-5 fluorescence recovery (Figures 9d and S11d), while **LB8** had no effect (Figure S11e). Our negative control, **LBc**, displayed no effect upon LDH reassociation (Figure S11f).

Finally, we investigated the ability of macrocycle **7** to disrupt the LDH oligomerization state. We therefore directly evaluated the impact of **7** on the native protein fluorescence. Strikingly, exposing human LDH-5 to **7** resulted in a concentration-dependent conversion of the LDH-5 fluorescence spectrum to the characteristic profile of the dimeric human LDH-Htr (Figure 9d). Normalization of the fluorescence intensity allowed approximation of the disruption ratio of LDH-5 upon exposure to increasing amount of **7** (Figure 9e). This disruptive effect (EC_{50} = 172 μM, $CI_{95\%}$ of 142−207 μM)) consistently matched the interaction previously observed using

https://dx.doi.org/10.1021/acs.jmedchem.9b01955
J. Med. Chem. 2020, 63, 4628−4643

MST (Figure 9e), indicating that the binding of 7 to the LDH tetramerization site promotes a disruption of the protein oligomeric state. Of note, macrocycle 7 did not induce a comparative decay of LDH-Htr fluorescence spectrum (Figure S11g).

Together, these results demonstrate that the designed cyclic peptides can target the tetramerization sites of LDHs by competing with the N-terminal domain of LDH-H and LDH-M monomers, leading to a destabilization and disruption of the tetrameric complexes. Moreover, these macrocycles can also interfere with the formation of LDH tetramers. These data also confirm that targeting of LDH highly conserved tetramerization site can lead to molecules interacting on both isoforms of the protein.

CONCLUSIONS

Despite a relatively low druggability, LDHs are attractive targets for anticancer therapy.[13,24,56] Targeting LDH oligomeric state using their tetramerization arms is an approach that has already been suggested,[42,57] as N-terminal arms are known to play an important role in tetramer assembly.[45] This strategy, however, was suffering from the lack of a well-defined starting point. In good agreement with previous reports that deletions of the last 5−10 amino acids are deleterious for enzymatic activity,[58] we demonstrated here that the epitope for LDH tetramerization arms is constituted by short N-terminal 8 amino acid α-helixes that project key lipophilic residues toward a highly lipophilic pocket. We also identified and characterized a family of octapeptides and related macrocycles that are, to our knowledge, the only ligands referenced for LDH tetramerization site. Among these molecules, the most potent analogue (7) can compete with the N-terminal tetramerization domain of LDHs, inducing a destabilization and a disruption of the protein complex. This stapled peptide also interfered with LDH tetramer formation.

Therefore, we believe that these short peptides and their stapled derivatives, especially macrocycle 7, represent a promising molecular framework for the further development of more potent LDH disruptors. They constitute, together with the dimeric forms of LDH, valuable pharmacological tools for the identification of new molecules interacting with LDH tetramerization sites.

EXPERIMENTAL SECTION

Chemicals and Peptides. All reagents were purchased from chemical suppliers and used without purification. Rabbit and recombinant human LDH-M were purchased respectively from Sigma-Aldrich and Abnova. Linear peptides used directly in biophysical experiments were purchased from Genecust, and linear peptides used for cysteine stapling were synthesized by solid-phase peptide synthesis. Lactam cyclic peptides were purchased from Proteogenix. Structure conformity and purity grade (>95%) were assessed by analytical high performance liquid chromatography (HPLC) analysis and mass spectrometry (MS) for both commercial and synthesized peptides. All peptides were amidated at their C-termini.

Peptide Synthesis. All peptides used for cysteine cross-linking procedures were synthesized on a 0.05 or 0.1 mmol scale using a Rink amide AM resin (Bachem) (substitution 0.5−1.2 mmol/g). Fluorenylmethyloxycarbonyl (Fmoc)-protected amino acids (5-fold excess) were activated with 1 equiv of hexafluorophosphate benzotriazole tetramethyluronium (HBTU) and 2 equiv of diisopropylethanolamine (DIPEA) (equivalent relative to the amino acid). Coupling was performed in *N*-methyl-2-pyrrolidone (NMP) for 60 min at room temperature. Fmoc deprotection was carried out using 20% piperidine in NMP for 10 min at room temperature. Side chain deprotection and simultaneous cleavage from the resin were achieved using a mixture of trifluoroacetic acid (TFA)/triisopropylsilane/water/thioanisole (90/2.5/2.5/5) at room temperature for 2 h. TFA was then evaporated under nitrogen flux, and the crude peptide was precipitated using ice cold diethyl ether. Crude peptides were then analyzed using an Agilent (1100 series) HPLC single quadrupole (InfinityLab, ESI+) system equipped with a Kinetex 5 μm EVO C18 (150 mm × 4,6 mm) and subsequently lyophilized for further use.

Synthesis of the Cross-Linked Peptides. *Stapling Using Bis-bromoxylene Derivatives.* Following described procedures,[48] the lyophilized crude peptide solution (~3 mg/mL, ~1.5 mM) in NH_4HCO_3 buffer (100 mM, pH = 8.0) was treated with tris(2-carboxyethyl)phosphine (TCEP; 1.5 equiv; 2.25 μL from 1 M solution in the same NH_4HCO_3 buffer), and stirred for 1 h at 700 rpm. The α,α'-bisbromoxylene in dimethylformamide (DMF; ~3 equiv; 100 μL from a 50 mM solution) was added to the solution and shaken for 2 h at 700 rpm. The reaction was quenched by adjusting the pH of the mixture to slightly acidic conditions through the addition of TFA (150 μL/mL). The crude mixture was then centrifuged at 10 000 rpm for 20 min. The supernatant was analyzed using an Agilent (1100 series) HPLC−MS single quadrupole (InfinityLab ESI+) system equipped with a Kinetex 5 μm EVO C18 (150 mm × 4.6 mm) and purified with a Kinetex 5 μm EVO C18 (150 mm × 21.2 mm) preparative HPLC. The mass of all peptides was verified by electrospray ionization (ESI)-MS, and purity (above 95%) was checked by analytical HPLC. Analysis and purification were performed using a distillated water + 0.1% TFA (buffer A) and acetonitrile + 0.1% TFA (buffer B) gradient. Initial HPLC conditions for routine analysis were 5% B + 95% A at a flow rate of 1 mL/min, followed by an increase of solution B to 80% in 15 min (5%/min). Purity check was performed at 210 nm using a routine broad gradient of 5% of B per min as well as a more focused gradient of 0.5−0.6% of B per min depending on the peptide structure. Overall purity was >95%. HPLC traces can be found in Supporting Information data.

Stapling Using Hexafluorobenzene. Following the described procedure,[59] to a lyophilized sample of peptide (~7.5 μmoles) was added 1.9 mL of 100 mM solution (~25 equiv) of hexafluorobenzene in DMF and 1.5 mL of 50 mM solution of Tris base in DMF. Solution was left under agitation at room temperature for 5 h. Resulting mixture was diluted with 2 times the volume of 0.1% TFA solution in water and subjected to analysis and purification on HPLC as described above.

High-Resolution Mass Spectroscopy Analysis. High-resolution mass spectroscopy (HRMS) analysis were performed on a LTQ-Orbitrap XL hybrid mass spectrometer (Thermo Fisher Scientific, Bremen, Germany). Data were acquired in full-scan MS positive ion mode. Analyzed mass ranged from 100 to 1500 m/z. The Orbitrap operated at 30 000 resolutions (fwhm definition). An external calibration was performed prior to data acquisition. Tuning of the electrospray ion source was performed accordingly. The following electrospray inlet conditions were used: flow rate, 100 μL min^{-1}; spray voltage, 5 kV; sheath gas (N_2) flow rate, 20 au; auxiliary gas (N_2) flow rate, 10 au; capillary temperature, 275 °C; capillary voltage, 45 V; tube lens, 80 V. HRMS analysis of the synthesized macrocycles can be found in Table S4.

Production and Purification of Human LDH Proteins. The *hLDHB* nucleotidic sequences used to produce full length, truncated, and variant LDH-H proteins inserted in a pET-28a expression vector were ordered from Genecust. NdeI and Bpu1102I restriction sites were used for sequence insertion and allowed for a N-terminal 6 histidine tag addition. Recombinant plasmids were then transformed in host bacterium *E. coli* Rosetta (DE3). Transformants were cultured in lysogeny broth (LB) medium with 50 μg/mL kanamycin and 34 μg/mL chloramphenicol at 37 °C until an optical density of 0.6 was reached. LDH expression was induced by the addition of 1 mM isopropyl-β-D-1-thiogalactopyranoside (IPTG) at 20 °C for 20 h. Then, cells were collected by centrifugation at 5000 rpm, 4 °C for 25 min. Pellets were suspended in a lysis buffer (Tris-HCl 50 mM, pH 8.5, $MgCl_2$ 10 mM, NaCl 300 mM, imidazole 5 mM, and glycerol

https://dx.doi.org/10.1021/acs.jmedchem.9b01955
J. Med. Chem. 2020, 63, 4628−4643

10%) and then disrupted by sonication, followed by a centrifugation at 4 °C, 10 000 rpm for 30 min. The insoluble fraction was discarded, and 1 μL of β-mercaptoethanol was added per mL of soluble fraction. The purification of recombinant proteins was performed using 1 mL of His-trap FF-crude columns (GE Healthcare) according to the manufacturer's instructions. Finally, protein concentrations were measured using the Bradford method with the Biorad protein assay kit, and sample homogeneity was assessed using sulfate−polyacrylamide gel electrophoresis (SDS−PAGE) with Coomassie brilliant blue as a staining agent.

Nuclear Magnetic Resonance. Human LDH-H (full length and truncated)-6His proteins for 1D NMR were expressed and purified from *E. coli*, as described above. All experiments were performed on a Bruker Ascend Avance III 600 MHz system equipped with a broadband cryoprobe (Bruker).

For WaterLOGSY NMR studies, samples were prepared in 10% D_2O containing 50 mM sodium phosphate buffer, pH 7.6, and 100 mM NaCl. The concentration of LDHs was ranging from 15 to 20 μM monomer. Ligand binding was detected using a WaterLOGSY ephogsygpno.2 avance-version sequence with a 1 s mixing time. Water signal suppression was achieved using an excitation-sculpting scheme, and a 50 ms spinlock was used to suppress protein background signals. For each experiment, 512 scans were collected to yield a 16K points free induction decay (FID). WaterLOGSY intensity was corrected by plotting the intensity difference of the ligand WaterLOGSY spectra recorded in the presence and absence of protein. For WaterLOGSY screening experiments, a correction factor was applied to account for slight concentration variations between samples. To do so, eight scans ^{1}H NMR spectra with 50 ms spinlock were recorded before WaterLOGSY experiments. The intensity ratio of the aliphatic region (0.700 ppm to 0.955 ppm) with and without protein was used as a correction. A threshold of 0.1, corresponding to a 10% decrease in the WaterLOGSY signal intensity between the spectra with and without protein, was set to discriminate between binders and non/weaker binders.

For 2D experiments, peptides were dissolved at 5 mM in a 50 mM phosphate buffer, pH 7.0, containing 100 mM NaCl, 1 mM trimethylsilylpropanoic acid (TSP), and 10% D_2O. For all experiments, water suppression was achieved using an excitation sculpting scheme. 4K time domain points and 256 increments were applied for all the 2D spectra. TOCSY experiments were performed using the homonuclear Hartman−Hahn transfer with the dipsi2 sequence and an 80 ms mixing time. An amount of 8 scans per spectrum, 4K time domain points, and 256 increments were recorded. ROESY experiments were performed using a 2D ROESY sequence with cw spinlock for mixing. A 400 ms mixing time was used, and 32 scans were acquired per line.

Circular Dichroism. Peptide solutions were prepared at precise concentrations ranging from 100 to 200 μM in a 10 mM sodium phosphate buffer, pH 7.6. Peptide solutions were prepared by considering the molecular weight of the TFA counterion and corrected for their concentration by HPLC−MS. CD analysis ranged from 183 to 260 nm and were performed at 25 °C on a JASCO J-715 spectropolarimeter. A Peltier instrument maintained the temperature stability during the analysis. Cells used were from Hellma Analytics and made of Quarts Suprasil with a 1 mm path length. Data were collected in millidegrees and further converted to mean residue ellipticity (MRE) following standard equation.

***In Silico* Evaluation.** Calculation of the free binding energy as well as modeling of the interacting peptides was performed using the MOE software (ChemComp) with the available crystallographic structure (PDB entry 1I0Z).[45] Tetrameric LDH-1 was generated from the PDB crystallographic structure using the MOE bioassembly tool. Truncated dimeric version of LDH-1 (LDH-Htr) was designed from the tetrameric complex by removing LDH-H subunits B and D as well as the N-terminal domain of subunits A and C (following usual nomenclature of LDH subunits).[57,60] **LB8** and cyclic peptide **1** were built directly in the tetramerization site by using the crystallographic structure of the N-terminal domain as a backbone. Protein and peptides structures were minimized using the MOE quickprep tool.

Sequence Alignment. Sequence alignment was performed with the Sequence Manipulation Suite Color Align Conservation tool.[61] Vertebrate LDH-H sequences were extracted in FASTA sequence from the Uniprot database (https://www.uniprot.org/). Groups of amino acids used for similarity calculation were the following: GAVLI, FYW, CM, ST, KRH, DENQ, and P. A threshold of 100% of similarity or identity was required for identity or similarity coloring to be added.

Size Exclusion Experiments. Size exclusion chromatography was performed using an ÄKTApure chromatography system (GE Healthcare) equipped with a Superdex 200 10/300 GL column (GE Healthcare) equilibrated with 50 mM sodium phosphate, pH 7.6, 100 mM NaCl assay buffer at 0.75 mL/min. Proteins were diluted to 15 μM in the assay buffer. The final injection volume was 500 μL. Prior to experiments, the column was equilibrated with 2× column volume of distillated and filtered H_2O, followed by 3× column volume of the filtered buffer. Molecular weight was determined using the Biorad gel filtration standard in the same assay buffer following the manufacturer's instructions.

Nano Differential Scanning Fluorimetry Experiments. *Variant Evaluation.* Solutions of proteins (LDH-Hfl, LDH-Htr or variants) stored in a 50 mM sodium phosphate, 100 mM NaCl, and 20% glycerol, pH 7.6, were evaluated on a Tycho NT.6 device (NanoTemper Technologies), using concentrations ranging from 15 to 20 μM. According to the standard manufacturer's procedures, samples were poured into capillaries and heated up to 95 °C in 3 min while following fluorescence emission at 330 and 350 nm. Melting temperatures were extracted from the derivative of the 350/330 nm fluorescence ratios upon increasing temperature.

Peptide Evaluation. Solutions of proteins (LDH-1, LDH-5 or LDH-Htr) were evaluated on a Tycho NT.6 device (NanoTemper Technologies), using concentrations ranging from 300 nM to 2.5 μM. Evaluations were run in a 50 mM sodium phosphate and 100 mM NaCl pH 7.6 buffer. According to standard manufacturer's procedures, samples were poured into capillaries and heated up to 95 °C in 3 min while following fluorescence emission at 330 and 350 nm. Melting temperatures were extracted from the derivative of the 350/330 nm fluorescence ratios upon increasing temperature.

Microscale Thermophoresis. MST measurements were performed on a Nanotemper Monolith NT.115 instrument (NanoTemper Technologies) using Red-dye-NHS fluorescent labeling. Each LDH sample, purified to homogeneity, was labeled with the Monolith Red-dye-NHS second generation labeling dye (Nanotemper Technologies), according to the supplied protocol. Measurements were performed in 50 mM sodium phosphate, pH 7.6, and 100 mM NaCl containing 0.05% Tween-20 in premium-treated capillaries (NanoTemper Technologies). The final concentrations of either labeled protein in the assay were 100 nM. The ligands (NADH and peptides) were titrated in 1:1 dilutions following the manufacturer's recommendations. All binding reactions were incubated for 5 min at room temperature after loading into capillaries. Experiments were performed in triplicates using 40% LED power, medium MST power, laser on time 20 s, and laser off time 3 s. Peptides were evaluated for their thermophoretic pattern, and K_d's were extracted from raw data at a 10−20 s MST on time according to the manufacturer's instructions. Regarding interaction of **7** with LDH-5, K_d was extracted from the raw fluorescence. A denaturation test was performed accordingly to the manufacturer's recommendation and excluded any nonspecific spectral interaction between **7** and the red-dye. All K_d's of interacting macrocycles and peptides were obtained in triplicate and corrected by taking into account the molecular weight of the TFA counterion. Peptide ATGKEKLI was used as a negative control and displayed no appreciable binding when compared to **LB8**. All MST binding curves to LDH-Htr can be found in Figure S12.

Spectrophotometric Experiments. All spectrophotometric experiments were performed with opaque 96-well plates using a Spectramax m2e spectrophotometer (Molecular Devices).

Kinetic Assays. The dehydrogenase reaction was run in the LDH-1 physiologically relevant lactate to pyruvate direction following the NADH fluorescence generated during lactate oxidation to pyruvate.

https://dx.doi.org/10.1021/acs.jmedchem.9b01955
J. Med. Chem. 2020, 63, 4628−4643

The progression of the reaction was monitored as the increase of fluorescence at 340/460 nm. The Michaelis–Menten K_M constant determination was performed using the GraphPad prism 7.0 software. Enzymatic reactions were performed in a solution containing phosphate buffer 100 mM at pH 8.0 to enhance lactate to pyruvate oxidation, EDTA 1 mM and 1 mM. Final protein concentration was 7.7 nM for LDH-Hfl and 13.5 nM for LDH-Htr. For NAD^+ K_m determination, concentrations of lactate were set to 20 mM for LDH-Hfl and 150 mM for LDH-Htr, while cofactor concentrations ranged from 1 μM to 5 mM for LDH-Hfl and from 50 μM to 10 mM for LDH-Htr. For lactate K_m determination, concentrations of NAD^+ were set to 1 mM while substrate concentrations ranged from 1 μM to 30 mM for LDH-Hfl and from 1 mM to 40 mM for LDH-Htr.

Intrinsic Fluorescence Assays. Full tryptophan fluorescence spectra were recorded using an excitation wavelength of 286 nm and recording the emission spectra from 320 to 400 nm at room temperature. Raw fluorescence of every experiments was further subtracted to a corresponding control experiment without the protein. Experiments were performed in a 50 mM sodium phosphate and 100 mM NaCl, pH 7.6, buffer. For LDH dissociation into subunits, increasing amounts of guadinidium·HCl were put in contact with the studied proteins (1.3 μM), and fluorescence spectra were recorded afterward. Guadinidium·HCl concentrations ranged from 0.3 to 2 M.

Denaturation Assays. Rabbit LDH-M commercial solution (Sigma-Aldrich) in an ammonium sulfate suspension (pH ~ 7, 3.2 M) was first diluted to 1 mg/mL in a solution of NaCl 200 mM and then dialyzed at 4 °C 2 × 2 h against 200 mM NaCl. The stock solution of 1 mg/mL was then diluted to 30 μg/mL (800 nM) in NaCl 200 mM to give the assay solution. Assay solution was mixed 1:1 with acetate–chloride buffer (20 mM acetic acid/acetate, 180 mM NaCI, 1 mM DTT, pH 5) and stored on ice for 30 min. Samples were then removed from ice and allowed to warm up for 2 min. The acidic solution was then diluted 1:1 with a 250 mM phosphate buffer (pH 7.6) containing or not the inhibitory peptide to yield a 7.5 μg/mL (200 nM) final concentration of reassociating LDH-M. Samples of the resulting solutions were then subjected to kinetic experiments of the recovery of intrinsic fluorescence (Exc = 286 nm, Em = 350 nm, 10 min, rt).

Statistics. All quantitative data are expressed as the mean ± SEM. Error bars are sometimes smaller than symbols. *n* refers to the total number of replicates per group. All experiments were repeated at least twice independently. Data were analyzed using the GraphPad Prism 7.0 software. Student's *t* test, one-way ANOVA, and two-way ANOVA were used where appropriate. $P < 0.05$ was considered to be statistically significant.

■ ASSOCIATED CONTENT

Supporting Information

The Supporting Information is available free of charge at https://pubs.acs.org/doi/10.1021/acs.jmedchem.9b01955.

Coordinates information for structure representation (PDB)

MOE information for LDH-1 coordinates (TXT)

Supporting figures and tables as well as HPLC traces of the purified macrocycles (PDF)

Molecular formula strings of cyclic peptides **1**–**12** (CSV)

■ AUTHOR INFORMATION

Corresponding Authors

Pierre Sonveaux – *Pole of Pharmacology and Therapeutics, Institut de Recherche Expérimentale et Clinique (IREC), Université Catholique de Louvain, B-1200 Brussels, Belgium;* Email: pierre.sonveaux@uclouvain.be

Raphaël Frédérick – *Louvain Drug Research Institute (LDRI), Université Catholique de Louvain, B-1200 Brussels, Belgium;* orcid.org/0000-0001-8119-1272; Email: raphael.frederick@uclouvain.be

Authors

Léopold Thabault – *Louvain Drug Research Institute (LDRI) and Pole of Pharmacology and Therapeutics, Institut de Recherche Expérimentale et Clinique (IREC), Université Catholique de Louvain, B-1200 Brussels, Belgium;* orcid.org/0000-0001-9501-6563

Lucie Brisson – *Pole of Pharmacology and Therapeutics, Institut de Recherche Expérimentale et Clinique (IREC), Université Catholique de Louvain, B-1200 Brussels, Belgium; INSERM UMR1069, Nutrition, Croissance et Cancer, Université François-Rabelais, F-37041 Tours, France*

Chiara Brustenga – *Louvain Drug Research Institute (LDRI), Université Catholique de Louvain, B-1200 Brussels, Belgium*

Santiago A. Martinez Gache – *VIB-VUB Center for Structural Biology, B-1050 Brussels, Belgium; Brussels Center for Redox Biology, B-1050 Brussels, Belgium; Structural Biology Brussels, Vrije Universiteit Brussel, B-1050 Brussels, Belgium*

Julien R. C. Prévost – *Louvain Drug Research Institute (LDRI), Université Catholique de Louvain, B-1200 Brussels, Belgium;* orcid.org/0000-0003-1569-8125

Arina Kozlova – *Louvain Drug Research Institute (LDRI), Université Catholique de Louvain, B-1200 Brussels, Belgium*

Quentin Spillier – *Louvain Drug Research Institute (LDRI) and Pole of Pharmacology and Therapeutics, Institut de Recherche Expérimentale et Clinique (IREC), Université Catholique de Louvain, B-1200 Brussels, Belgium*

Maxime Liberelle – *Louvain Drug Research Institute (LDRI), Université Catholique de Louvain, B-1200 Brussels, Belgium*

Zohra Benyahia – *Pole of Pharmacology and Therapeutics, Institut de Recherche Expérimentale et Clinique (IREC), Université Catholique de Louvain, B-1200 Brussels, Belgium*

Joris Messens – *VIB-VUB Center for Structural Biology, B-1050 Brussels, Belgium; Brussels Center for Redox Biology, B-1050 Brussels, Belgium; Structural Biology Brussels, Vrije Universiteit Brussel, B-1050 Brussels, Belgium*

Tamara Copetti – *Pole of Pharmacology and Therapeutics, Institut de Recherche Expérimentale et Clinique (IREC), Université Catholique de Louvain, B-1200 Brussels, Belgium*

Complete contact information is available at: https://pubs.acs.org/10.1021/acs.jmedchem.9b01955

Author Contributions

P.S. and R.F. are co-senior authors. L.T., P.S., and R.F. designed the research. L.T., L.B., C.B., S.A.M.G., and Z.B. performed the research experiments. L.T., S.A.M.G., J.R.C.P., A.K., Q.S., M.L., T.C., and J.M. analyzed the data. L.T., J.R.C.P., A.K., and Q.S. set up the experimental methods, and L.T., P.S., and R.F. wrote the paper.

Notes

The authors declare the following competing financial interest(s): L.T., L.B., T.C., P.S., and R.F. are inventors of European Patent Application EP19172347.7, Lactate dehydrogenase inhibitor polypeptides for use in treatment of cancer. Authors declare no other conflicts of interest.

■ ACKNOWLEDGMENTS

This work was supported by ERC independent researcher Starting Grant 243188, TUMETABO, the Belgian Science Policy Office (Belspo; Interuniversity Attraction Pole Grant

P7/03), the French Community of Belgium (ARC 14/19-058), the Belgian Fonds National de la Recherche Scientifique (F.R.S.-FNRS; Grants 3.4575.11, 2.5025.12, and 31288018), the Belgian Fondation contre le Cancer (Fundamental Research Grant FAF-F/2018/1282), and the Télévie (Grants 7.4611.11, 7.4548.13, 7.4507.14, and 7.8504.18). L.T. is a Ph.D. Fellow, and P.S. is a Senior Research Associate of the F.R.S.-FNRS. The authors thank Marie-France Hérent, Morgane Tardy, Marie-Joséphine Fontenille, Fabien Rodriguez, Thibaut Vazeille, Bouazza Es Saadi, Esra Yildiz, and Claudia Tavernier for excellent technical assistance. The authors thank Dr. Jamal El Bakali, Severine Ravez, Nicolas Joudiou, Vincent Stroobant, and Didier Colau for fruitful discussions. Funding sources had no role in study design, data collection and interpretation, or the decision to submit the work for publication.

■ ABBREVIATIONS USED

LDH, lactate dehydrogenase; LDH-H, lactate dehydrogenase heart isozyme; OXPHOS, oxidative phosphorylation; TCA, tricarboxylic acid; LDH-M, lactate dehydrogenase muscle isozyme; LDH-1, lactate dehydrogenase heart isozyme homotetramer; LDH-5, lactate dehydrogenase muscle isozyme homotetramer; *LDHA*, lactate dehydrogenase M gene; *LDHB*, lactate dehydrogenase H gene; V_{max}, maximum velocity; NCBI, National Center for Biotechnology Information; BLAST, basic local alignment search tool; vdW, van der Waals; HRE, hypoxia-responsive element; LDH-Hfl, full length lactate dehydrogenase heart isozyme; LDH-Htr, truncated lactate dehydrogenase heart isozyme; kDa, kilodalton; MST, microscale thermophoresis; nanoDSF, nano differential scanning fluorimetry; RFU, relative fluorescent unit; Rv, retention volume; K_d, dissociation constant; k_{cat}, catalytic constant; WaterLOGSY, water-ligand observed via gradient spectroscopy; TOCSY, total correlated spectroscopy; ROESY, rotating-frame nuclear Overhauser effect correlation spectroscopy; MOE, Molecular Operating Environment; Gdn.HCl, guadinidium chloride; T_m, melting temperature; ΔT_m, thermal shift; λ_{exc}, wavelength of excitation; λ_{em}, wavelength of emission; λ_{max}, wavelength of maximal emission; SEM, standard error of the mean; Aib, aminoisobutyric acid; TFE, trifluoroethanol; CI95%, confidence interval at 95%; rLDH-5, rabbit lactate dehydrogenase muscle isozyme homotetramer; rLDH-M, rabbit lactate dehydrogenase muscle isozyme; Fmoc, fluorenylmethyloxycarbonyl; HBTU, hexafluorophosphate benzotriazole tetramethyluronium; DIPEA, diisopropylethanolamine; NMP, *N*-methyl-2-pyrrolidone; TFA, trifluoroacetic acid; ESI+, electrospray ionization positive mode; TCEP, tris(2-carboxyethyl)phosphine; DMF, dimethylformamide; HPLC−MS, high performance liquid chromatography−mass spectrometry; fwhm, full width at half-maximum; IPTG, isopropyl-β-D-1-thiogalactopyranoside; TSP, trimethylsilylpropanoic acid; MRE, mean residue ellipticity; NHS, *N*-hydroxysuccinimide; LED, light-emitting diode

■ REFERENCES

(1) Semenza, G. L.; Roth, P. H.; Fang, H. M.; Wang, G. L. Transcriptional Regulation of Genes Encoding Glycolytic Enzymes by Hypoxia-Inducible Factor 1. *J. Biol. Chem.* **1994**, *269*, 23757−23763.
(2) Warburg, O.; Wind, F.; Negelein, N. The Metabolism of Tumours in the Body. *J. Gen. Physiol.* **1927**, *8*, 519−530.
(3) Sonveaux, P.; Végran, F.; Schroeder, T.; Wergin, M. C.; Verrax, J.; Rabbani, Z. N.; De Saedeleer, C. J.; Kennedy, K. M.; Diepart, C.; Jordan, B. F.; Kelley, M. J.; Gallez, B.; Wahl, M. L.; Feron, O.; Dewhirst, M. W. Targeting Lactate-Fueled Respiration Selectively Kills Hypoxic Tumor Cells in Mice. *J. Clin. Invest.* **2008**, *118*, 3930−3942.
(4) Whitaker-Menezes, D.; Martinez-Outschoorn, U. E.; Lin, Z.; Ertel, A.; Flomenberg, N.; Witkiewicz, A. K.; Birbe, R.; Howell, A.; Pavlides, S.; Gandara, R.; Pestell, R. G.; Sotgia, F.; Philp, N. J.; Lisanti, M. P. Evidence for a Stromal-Epithelial "Lactate Shuttle" in Human Tumors. *Cell Cycle* **2011**, *10*, 1772−1783.
(5) de Saedeleer, C. J.; Copetti, T.; Porporato, P. E.; Verrax, J.; Feron, O.; Sonveaux, P. Lactate Activates HIF-1 in Oxidative but Not in Warburg-Phenotype Human Tumor Cells. *PLoS One* **2012**, *7*, No. e46571.
(6) Beckert, S.; Farrahi, F.; Aslam, R. S.; Scheuenstuhl, H.; Königsrainer, A.; Hussain, M. Z.; Hunt, T. K. Lactate Stimulates Endothelial Cell Migration. *Wound Repair Regen.* **2006**, *14*, 321−324.
(7) Végran, F.; Boidot, R.; Michiels, C.; Sonveaux, P.; Feron, O. Lactate Influx through the Endothelial Cell Monocarboxylate Transporter MCT1 Supports an NF-KB/IL-8 Pathway That Drives Tumor Angiogenesis. *Cancer Res.* **2011**, *71*, 2550−2560.
(8) Izumi, H.; Takahashi, M.; Uramoto, H.; Nakayama, Y.; Oyama, T.; Wang, K. Y.; Sasaguri, Y.; Nishizawa, S.; Kohno, K. Monocarboxylate Transporters 1 and 4 Are Involved in the Invasion Activity of Human Lung Cancer Cells. *Cancer Sci.* **2011**, *102*, 1007−1013.
(9) Colen, C. B.; Shen, Y.; Ghoddoussi, F.; Yu, P.; Francis, T. B.; Koch, B. J.; Monterey, M. D.; Galloway, M. P.; Sloan, A. E.; Mathupala, S. P. Metabolic Targeting of Lactate Efflux by Malignant Glioma Inhibits Invasiveness and Induces Necrosis: An in Vivo Study. *Neoplasia* **2011**, *13*, 620−632.
(10) Colegio, O. R.; Chu, N. Q.; Szabo, A. L.; Chu, T.; Rhebergen, A. M.; Jairam, V.; Cyrus, N.; Brokowski, C. E.; Eisenbarth, S. C.; Phillips, G. M.; Cline, G. W.; Phillips, A. J.; Medzhitov, R. Functional Polarization of Tumour-Associated Macrophages by Tumour-Derived Lactic Acid. *Nature* **2014**, *513*, 559−563.
(11) Doherty, J. R.; Cleveland, J. L. Targeting Lactate Metabolism for Cancer Therapeutics. *J. Clin. Invest.* **2013**, *123*, 3685−3692.
(12) Brisson, L.; Bański, P.; Sboarina, M.; Dethier, C.; Danhier, P.; Fontenille, M.-J.; Van Hée, V. F.; Vazeille, T.; Tardy, M.; Falces, J.; Bouzin, C.; Porporato, P. E.; Frédérick, R.; Michiels, C.; Copetti, T.; Sonveaux, P. Lactate Dehydrogenase B Controls Lysosome Activity and Autophagy in Cancer. *Cancer Cell* **2016**, *30*, 418−431.
(13) Fiume, L.; Manerba, M.; Vettraino, M.; Di Stefano, G. Inhibition of Lactate Dehydrogenase Activity as an Approach to Cancer Therapy. *Future Med. Chem.* **2014**, *6*, 429−445.
(14) Payen, V. L.; Brisson, L.; Dewhirst, M. W.; Sonveaux, P. Common Responses of Tumors and Wounds to Hypoxia. *Cancer J.* **2015**, *21*, 75−87.
(15) Semenza, G. L.; Jiang, B.-H.; Leung, S. W.; Passantino, R.; Concordet, J.-P.; Maire, P.; Giallongo, A. Hypoxia Response Elements in the Aldolase A, Enolase 1, and Lactate Dehydrogenase A Gene Promoters Contain Essential Binding Sites for Hypoxia-Inducible Factor 1. *J. Biol. Chem.* **1996**, *271*, 32529−32537.
(16) Strickaert, A.; Saiselet, M.; Dom, G.; De Deken, X.; Dumont, J. E.; Feron, O.; Sonveaux, P.; Maenhaut, C. Cancer Heterogeneity Is Not Compatible with One Unique Cancer Cell Metabolic Map. *Oncogene* **2017**, *36*, 2637−2642.
(17) Everse, J.; Kaplan, N. O. Lactate Dehydrogenases: Structure and Function. *Adv. Enzymol. Relat. Areas Mol. Biol.* **1973**, *37*, 61−133.
(18) Eszes, C. M.; Sessions, R. B.; Clarke, A. R.; Moreton, K. M.; Holbrook, J. J. Removal of Substrate Inhibition in a Lactate Dehydrogenase from Human Muscle by a Single Residue Change. *FEBS Lett.* **1996**, *399*, 193−197.
(19) Hewitt, C. O.; Eszes, C. M.; Sessions, R. B.; Moreton, K. M.; Dafforn, T. R.; Takei, J.; Dempsey, C. E.; Clarke, A. R.; Holbrook, J. J. A General Method for Relieving Substrate Inhibition in Lactate Dehydrogenases. *Protein Eng., Des. Sel.* **1999**, *12*, 491−496.
(20) Tanaka, M.; Nakamura, F.; Mizokawa, S.; Matsumura, A.; Matsumura, K.; Murata, T.; Shigematsu, M.; Kageyama, K.; Ochi, H.;

https://dx.doi.org/10.1021/acs.jmedchem.9b01955
J. Med. Chem. 2020, 63, 4628−4643

Watanabe, Y. Role of Lactate in the Brain Energy Metabolism: Revealed by Bioradiography. *Neurosci. Res.* **2004**, *48*, 13−20.
(21) Kanno, T.; Sudo, K.; Maekawa, M.; Nishimura, Y.; Ukita, M.; Fukutake, K. Lactate Dehydrogenase M-Subunit Deficiency: A New Type of Hereditary Exertional Myopathy. *Clin. Chim. Acta* **1988**, *173*, 89−98.
(22) Wakabayashi, H.; Tsuchiya, M.; Yoshino, K.; Kaku, K.; Shigei, H. Hereditary Deficiency of Lactate Dehydrogenase H-Subunit. *Intern. Med.* **1996**, *35*, 550−554.
(23) Granchi, C.; Bertini, S.; Macchia, M.; Minutolo, F. Inhibitors of Lactate Dehydrogenase Isoforms and Their Therapeutic Potentials. *Curr. Med. Chem.* **2010**, *17*, 672−697.
(24) Rani, R.; Kumar, V. Recent Update on Human Lactate Dehydrogenase Enzyme 5 (HLDH5) Inhibitors: A Promising Approach for Cancer Chemotherapy. *J. Med. Chem.* **2016**, *59*, 487−496.
(25) Altschul, S. F.; Gish, W.; Miller, W.; Myers, E. W.; Lipman, D. J. Basic Local Alignment Search Tool. *J. Mol. Biol.* **1990**, *215*, 403−410.
(26) Labadie, S.; Dragovich, P. S.; Chen, J.; Fauber, B. P.; Boggs, J.; Corson, L. B.; Ding, C. Z.; Eigenbrot, C.; Ge, H.; Ho, Q.; Lai, K. W.; Ma, S.; Malek, S.; Peterson, D.; Purkey, H. E.; Robarge, K.; Salphati, L.; Sideris, S.; Ultsch, M.; Vanderporten, E.; Wei, B.; Xu, Q.; Yen, I.; Yue, Q.; Zhang, H.; Zhang, X.; Zhou, A. Optimization of 5-(2,6-Dichlorophenyl)-3-Hydroxy-2- Mercaptocyclohex-2-Enones as Potent Inhibitors of Human Lactate Dehydrogenase. *Bioorg. Med. Chem. Lett.* **2015**, *25*, 75−82.
(27) Billiard, J.; Dennison, J. B.; Briand, J.; Annan, R. S.; Chai, D.; Colón, M.; Dodson, C. S.; Gilbert, S. A.; Greshock, J.; Jing, J.; Lu, H.; McSurdy-Freed, J. E.; Orband-Miller, L. A.; Mills, G. B.; Quinn, C. J.; Schneck, J. L.; Scott, G. F.; Shaw, A. N.; Waitt, G. M.; Wooster, R. F.; Duffy, K. J. Quinoline 3-Sulfonamides Inhibit Lactate Dehydrogenase A and Reverse Aerobic Glycolysis in Cancer Cells. *Cancer Metab.* **2013**, *1*, 19.
(28) Rai, G.; Brimacombe, K. R.; Mott, B. T.; Urban, D. J.; Hu, X.; Yang, S. M.; Lee, T. D.; Cheff, D. M.; Kouznetsova, J.; Benavides, G. A.; Pohida, K.; Kuenstner, E. J.; Luci, D. K.; Lukacs, C. M.; Davies, D. R.; Dranow, D. M.; Zhu, H.; Sulikowski, G.; Moore, W. J.; Stott, G. M.; Flint, A. J.; Hall, M. D.; Darley-Usmar, V. M.; Neckers, L. M.; Dang, C. V.; Waterson, A. G.; Simeonov, A.; Jadhav, A.; Maloney, D. J. Discovery and Optimization of Potent, Cell-Active Pyrazole-Based Inhibitors of Lactate Dehydrogenase (LDH). *J. Med. Chem.* **2017**, *60*, 9184−9204.
(29) Ždralević, M.; Brand, A.; Di Ianni, L.; Dettmer, K.; Reinders, J.; Singer, K.; Peter, K.; Schnell, A.; Bruss, C.; Decking, S.-M.; Koehl, G.; Felipe-Abrio, B.; Durivault, J.; Bayer, P.; Evangelista, M.; O'Brien, T.; Oefner, P. J.; Renner, K.; Pouysségur, J.; Kreutz, M. Double Genetic Disruption of Lactate Dehydrogenases A and B Is Required to Ablate the 'Warburg Effect' Restricting Tumor Growth to Oxidative Metabolism. *J. Biol. Chem.* **2018**, *293*, 15947−15961.
(30) Purkey, H. E.; Robarge, K.; Chen, J.; Chen, Z.; Corson, L. B.; Ding, C. Z.; DiPasquale, A. G.; Dragovich, P. S.; Eigenbrot, C.; Evangelista, M.; Fauber, B. P.; Gao, Z.; Ge, H.; Hitz, A.; Ho, Q.; Labadie, S. S.; Lai, K. W.; Liu, W.; Liu, Y.; Li, C.; Ma, S.; Malek, S.; O'Brien, T.; Pang, J.; Peterson, D.; Salphati, L.; Sideris, S.; Ultsch, M.; Wei, B.; Yen, I.; Yue, Q.; Zhang, H.; Zhou, A. Cell Active Hydroxylactam Inhibitors of Human Lactate Dehydrogenase with Oral Bioavailability in Mice. *ACS Med. Chem. Lett.* **2016**, *7*, 896−901.
(31) Ward, R. A.; Brassington, C.; Breeze, A. L.; Caputo, A.; Critchlow, S.; Davies, G.; Goodwin, L.; Hassall, G.; Greenwood, R.; Holdgate, G. A.; Mrosek, M.; Norman, R. A.; Pearson, S.; Tart, J.; Tucker, J. A.; Vogtherr, M.; Whittaker, D.; Wingfield, J.; Winter, J.; Hudson, K. Design and Synthesis of Novel Lactate Dehydrogenase A Inhibitors by Fragment-Based Lead Generation. *J. Med. Chem.* **2012**, *55*, 3285−3306.
(32) Kohlmann, A.; Zech, S. G.; Li, F.; Zhou, T.; Squillace, R. M.; Commodore, L.; Greenfield, M. T.; Lu, X.; Miller, D. P.; Huang, W. S.; Qi, J.; Thomas, R. M.; Wang, Y.; Zhang, S.; Dodd, R.; Liu, S.; Xu, R.; Xu, Y.; Miret, J. J.; Rivera, V.; Clackson, T.; Shakespeare, W. C.; Zhu, X.; Dalgarno, D. C. Fragment Growing and Linking Lead to Novel Nanomolar Lactate Dehydrogenase Inhibitors. *J. Med. Chem.* **2013**, *56*, 1023−1040.
(33) Rao, S. T.; Rossmann, M. G. Comparison of Super-Secondary Structures in Proteins. *J. Mol. Biol.* **1973**, *76*, 241−256.
(34) Opitz, U.; Rudolph, R.; Jaenicke, R.; Ericsson, L.; Neurath, H. Proteolytic Dimers of Porcine Muscle Lactate Dehydrogenase: Characterization, Folding, and Reconstitution of the Truncated and Nicked Polypeptide Chain. *Biochemistry* **1987**, *26*, 1399−1406.
(35) Wang, X.-C.; Jiang, L.; Zhou, H.-M. Minimal Functional Unit of Lactate Dehydrogenase. *J. Protein Chem.* **1997**, *16*, 227−231.
(36) Shahian, T.; Lee, G. M.; Lazic, A.; Arnold, L. A.; Velusamy, P.; Roels, C. M.; Guy, R. K.; Craik, C. S. Inhibition of a Viral Enzyme by a Small-Molecule Dimer Disruptor. *Nat. Chem. Biol.* **2009**, *5*, 640−646.
(37) Cardinale, D.; Salo-Ahen, O. M.; Ferrari, S.; Ponterini, G.; Cruciani, G.; Carosati, E.; Tochowicz, A. M.; Mangani, S.; Wade, R. C.; Costi, M. . Homodimeric Enzymes as Drug Targets. *Curr. Med. Chem.* **2010**, *17*, 826−846.
(38) Ruiz-Santaquiteria, M.; Sánchez-Murcia, P. A.; Toro, M. A.; de Lucio, H.; Gutiérrez, K. J.; de Castro, S.; Carneiro, F. A. C.; Gago, F.; Jiménez-Ruiz, A.; Camarasa, M. J.; Velázquez, S. First Example of Peptides Targeting the Dimer Interface of Leishmania Infantum Trypanothione Reductase with Potent in Vitro Antileishmanial Activity. *Eur. J. Med. Chem.* **2017**, *135*, 49−59.
(39) He, M. M.; Smith, A. S.; Oslob, J. D.; Flanagan, W. M.; Braisted, A. C.; Whitty, A.; Cancilla, M. T.; Wang, J.; Lugovskoy, A. A.; Yoburn, J. C.; Fung, A. D.; Farrington, G.; Eldredge, J. K.; Day, E. S.; Cruz, L. A.; Cachero, T. G.; Miller, S. K.; Friedman, J. E.; Choong, I. C.; Cunningham, B. C. Small-Molecule Inhibition of TNF-α. *Science* **2005**, *310*, 1022−1025.
(40) Adams, M. J.; Ford, G. C.; Koekoek, R.; Lentz, P. J.; McPherson, A.; Rossmann, M. G.; Smiley, I. E.; Schevitz, R. W.; Wonacott, A. J. Structure of Lactate Dehydrogenase at 2.8 A. *Nature* **1970**, *227*, 1098−1103.
(41) Girg, R.; Rudolph, R.; Jaenicke, R. Limited Proteolysis of Porcine-Muscle Lactic Dehydrogenase by Thermolysin during Reconstitution Yields Dimers. *Eur. J. Biochem.* **1981**, *119*, 301−305.
(42) Döbeli, H.; Gillessen, D.; Lergier, W.; Van Dijk, A.; Schoenenberger, G. A. Inhibition of the Reactivation of Acid-Dissociated Lactate Dehydrogenase Isoenzymes by Their Amino-terminal CNBr Fragments. *Peptides* **1987**, *8*, 773−778.
(43) Salthe, S. N.; Chilson, O. P.; Kaplan, N. O. Hybridization of Lactic Dehydrogenase in Vivo and in Vitro. *Nature* **1965**, *207*, 723−726.
(44) Dalvit, C.; Pevarello, P.; Tatò, M.; Veronesi, M.; Vulpetti, A.; Sundström, M. Identification of Compounds with Binding Affinity to Proteins via Magnetization Transfer from Bulk Water. *J. Biomol. NMR* **2000**, *18*, 65−68.
(45) Read, J. A.; Winter, V. J.; Eszes, C. M.; Sessions, R. B.; Brady, R. L. Structural Basis for Altered Activity of M-and H-isozyme Forms of Human Lactate Dehydrogenase. *Proteins: Struct., Funct., Genet.* **2001**, *43*, 175−185.
(46) Appella, E.; Markert, C. L. Dissociation of Lactate Dehydrogenase into Subunits with Guanidine Hydrochloride. *Biochem. Biophys. Res. Commun.* **1961**, *6*, 171−176.
(47) Hill, T. A.; Shepherd, N. E.; Diness, F.; Fairlie, D. P. Constraining Cyclic Peptides to Mimic Protein Structure Motifs. *Angew. Chem., Int. Ed.* **2014**, *53*, 13020−13041.
(48) Jo, H.; Meinhardt, N.; Wu, Y.; Kulkarni, S.; Hu, X.; Low, K. E.; Davies, P. L.; Degrado, W. F.; Greenbaum, D. C. Development of Alpha-Helical Calpain Probes by Mimicking a Natural Protein-Protein Interaction. *J. Am. Chem. Soc.* **2012**, *134*, 17704−17713.
(49) Hoang, H. N.; Driver, R. W.; Beyer, R. L.; Hill, T. A.; D. de Araujo, A.; Plisson, F.; Harrison, R. S.; Goedecke, L.; Shepherd, N. E.; Fairlie, D. P. Helix Nucleation by the Smallest Known α-Helix in Water. *Angew. Chem., Int. Ed.* **2016**, *55*, 8275−8279.
(50) Seetoh, W. G.; Abell, C. Disrupting the Constitutive, Homodimeric Protein-Protein Interface in CK2β Using a Biophysical

https://dx.doi.org/10.1021/acs.jmedchem.9b01955
J. Med. Chem. 2020, 63, 4628−4643

Fragment-Based Approach. *J. Am. Chem. Soc.* **2016**, *138*, 14303−14311.
(51) Gervais, V.; Muller, I.; Mari, P. O.; Mourcet, A.; Movellan, K. T.; Ramos, P.; Marcoux, J.; Guillet, V.; Javaid, S.; Burlet-Schiltz, O.; Czaplicki, G.; Milon, A.; Giglia-Mari, G. Small Molecule-Based Targeting of TTD-A Dimerization to Control TFIIH Transcriptional Activity Represents a Potential Strategy for Anticancer Therapy. *J. Biol. Chem.* **2018**, *293*, 14974−14988.
(52) Nordhoff, A.; Tziatzios, C.; Van Den Broek, J. A.; Schott, M. K.; Kalbitzer, H. R.; Becker, K.; Schubert, D.; Schirmer, R. H. Denaturation and Reactivation of Dimeric Human Glutathione Reductase: An Assay for Folding Inhibitors. *Eur. J. Biochem.* **1997**, *245*, 273−282.
(53) Yamamoto, S.; Storey, K. B. Dissociation-Association of Lactate Dehydrogenase Isozymes: Influences on the Formation of Tetramers versus Dimers of M4-LDH and H4-LDH. *Int. J. Biochem.* **1988**, *20*, 1261−1265.
(54) Chilson, O. P.; Chilson, A. E. Perturbation of Folding and Reassociation of Lactate Dehydrogenase by Proline and Trimethylamine Oxide. *Eur. J. Biochem.* **2003**, *270*, 4823−4834.
(55) Lovell, S. J.; Winzor, D. J. Effects of Phosphate on the Dissociation and Enzymic Stability of Rabbit Muscle Lactate Dehydrogenase. *Biochemistry* **1974**, *13*, 3527−3531.
(56) Augoff, K.; Hryniewicz-Jankowska, A.; Tabola, R. Lactate Dehydrogenase 5: An Old Friend and a New Hope in the War on Cancer. *Cancer Lett.* **2015**, *358*, 1−7.
(57) Jafary, F.; Ganjalikhany, M. R.; Moradi, A.; Hemati, M.; Jafari, S. Novel Peptide Inhibitors for Lactate Dehydrogenase A (LDHA): A Survey to Inhibit LDHA Activity via Disruption of Protein-Protein Interaction. *Sci. Rep.* **2019**, *9*, 4686.
(58) Zheng, Y.; Guo, S.; Guo, Z.; Wang, X. Effects of N-Terminal Deletion Mutation on Rabbit Muscle Lactate Dehydrogenase. *Biochemistry* **2004**, *69*, 401−406.
(59) Spokoyny, A. M.; Zou, Y.; Ling, J. J.; Yu, H.; Lin, Y. S.; Pentelute, B. L. A Perfluoroaryl-Cysteine SNAr Chemistry Approach to Unprotected Peptide Stapling. *J. Am. Chem. Soc.* **2013**, *135*, 5946−5949.
(60) Schmidt, R. K.; Gready, J. E. Molecular Dynamics Simulations of L-Lactate Dehydrogenase: Conformation of a Mobile Loop and Influence of the Tetrameric Protein Environment. *J. Mol. Model.* **1999**, *5*, 153−168.
(61) Stothard, P. The Sequence Manipulation Suite: JavaScript Programs for Analyzing and Formatting Protein and DNA Sequences. *BioTechniques* **2000**, *28*, 1102−1104.

https://dx.doi.org/10.1021/acs.jmedchem.9b01955
J. Med. Chem. 2020, 63, 4628−4643